



“New mechanisms and concepts for exploiting electroactive
Polymers for Wave Energy Conversion”

FP7-ENERGY-2012-1-2STAGE
FUTURE EMERGING TECHNOLOGIES

Grant Agreement N. 309139

Wave tank tests of intermediate scale PolyWEC-unit device in operational conditions			
Deliverable No.	4.3		
WP No.	4	WP Title	Tank tests
Task	4.2	Task Title	Tank testing in operational conditions
Task	4.3	Task Title	Testing in exceptional conditions
Nature (R: Report, P: Prototype, O: Other)	R		
Dissemination level (PU, PP, RE, CO)	PU		
Lead beneficiary:	UEDIN		
Authors List:	Giacomo Moretti, Gastone Pietro Rosati Papini (SSSA) Francesco Damiani, Luca Daniele, Marco Fontana (SSSA), Rocco Vertechy (UNIBO), David Forehand (UEDIN), Jeffrey Steynor, Tom Davey (FloWave)		
Status (F: final; D: draft; RD: revised draft):	F		
File Name:	D43_Intermediate_scale_testing_FINAL.pdf		
Due Delivery Date:	M45		
Actual Delivery Date:	M51		

Version History table

Version no.	Dates and comments
1	Aug 2016 Frist draft
2	Oct 2016 Integration of data processing
3	Jan 2017 Finalization of model validation
4	
5	

INDEX

INDEX	3
Executive summary	4
1. INTRODUCTION.....	6
2. EXPERIMENTAL SETUP, PROCEDURE AND DATA PROCESSING.....	9
2.1 Prototype design.....	9
2.2 Prototype construction	10
2.3 Control and electric layout	11
2.3.1 Generated power measurement	14
3 Data processing and results	15
3.1 Hydrodynamic tests (fully open collector).....	16
3.2 Mechanical tests with idle CD-DEG.....	17
3.3 Electric generation tests results	18
3.3.1 Regular waves performance assessment	20
3.3.2 Irregular waves performance assessment	21
3.4 Survivability tests	23
3.5 Tests with waves and currents.....	24
4. Models Validation	25
4.1 Poly-U-OWC mathematical model.....	25
4.1.1 Collector hydrodynamic model	25
.....	26
4.1.2 DEG electro-mechanical model	29
4.1.3 Air chamber model	30
4.2 Model validation	31
4.2.1 Hydrodynamic model validation	31
4.2.2 U-OWC + DEG mechanical model validation	33
4.2.3 Wave-to-wire hydro-electro-elastic model validation.....	37
4.2.4 Collector + DEG + open air chamber model validation	40
xx. CONCLUSIONS AND FUTURE WORKS.....	41
x.1 Conclusions	41
References.....	43

EXECUTIVE SUMMARY

This deliverable reports on a set of wave tank tests conducted in the framework of the project PolyWEC, funded by the European Commission under the FP7-Energy programme.

In previous test sessions different wave energy converters equipped with Dielectric Elasomer Generators (DEGs) devices were successfully tested at smaller scale level. Specifically:

- A first set of tests were conducted at very small scale (1:70 – 1:80) on a laboratory setup that was purposely designed and built. These tests made it possible to characterize the performances of the DEG-PTO system and verify the modelling approach (described in D1.2).
- Two sets of tests were conducted in the wave flume facility available at University of Edinburgh with 2D demonstrating prototypes: (1) a very preliminary OWC system was employed at first to demonstrate the feasibility of the concept and to get an understanding of several experimental issues (this system featured sub-optimal global performances); (2) a second set of tests were dedicated to the characterization of an improved prototype obtained through a thorough design process that provided largely superior performances with respect to the first system.
- A further test session has been conducted in the FloWave facility, in Edinburgh, employing a representative OWC floating point absorber device that was inspired by the specific design proposed by Sendekia Company [17]. These tests made it possible to verify the performance of the system with a more realistic layout.
- A first prototype of direct contact device (i.e. device in which the DEG is in direct contact with water) has been tested in the Edinburgh Curved tank in order to verify the assumed modelling approach and to asses a novel conceptual strategy that made it possible to implement a simple strategy to tune the dynamic response of the WEC.

In the last test session reported here, a new concept of DEG-WEC has been introduced and built at an intermediate scale (1:25-1:30). Tests were performed in the Flowave facility in Edinburgh. The device is a point absorber OWC system that features a particular shape based on axisymmetric dual-tube structure for the submerged collector (that is named U-OWC). This solution makes it possible to obtain a high added mass and a relevant power capture for the WEC maintaining a sufficiently compact shape of the whole device.

As in the previous test sessions, the developed WEC prototype is equipped with a fully functional PTO system that is actually able to absorb energy from waves and convert it into DC electrical energy.

In compliance with the design guidelines that have been identified during the project and described in the deliverable D3.4, the device was designed according to an integrated procedure that considers from the beginning the effects of primary interface and PTO on the overall system response. This approach made it possible to achieve a tuned dynamic response with rather elevated performance.

Tank tests have been conducted in operational and exceptional conditions.

Operational tests included monochromatic and panchromatic wave trains at different frequencies and different wave heights. The satisfactory matching between the measured results and predictive mathematical models make it possible to validate the employed strategy for the design of the system.

Beside the verification of models, during the test the PTO was able to output a significant amount of power, in the order of 3 W (corresponding to about 250-400kW in real scale), providing a demonstration of a first step-up in the scalability of the system and validating the scaling rules defined in D3.4.

As regards the experiments in exceptional sea conditions, the following tests have been performed:

- A set of survivability tests under extreme seas with waves. In these tests a new conceptual strategy that makes it possible to reduce extreme loads on the PTO has been successfully demonstrated;
- A set of tests with combined wave and current have been conducted in order to verify the (reduced) influence of currents on the system performances.

List of acronyms:

CD-DEG: Circular Diaphragm Dielectric Elastomer Generator (to refer to the PolyOWC PTO)
DE: Dielectric Elastomers;
DEG: Dielectric Elastomer Generator (to refer to the whole generator);
ECC: Energy Conversion Cycle;
HV: High Voltage;
OWC: Oscillating Water Column;
Poly-OWC: Polymeric Oscillating Water column (based on dielectric elastomer transducers);
PTO: Power Take Off
WEC: Wave Energy Converter;

1. INTRODUCTION

First tests on PolyWEC devices have been reported in Deliverable D4.1 [1]. Yet at that level, attention has been focused on a specific PolyWEC concept, namely, the PolyOWC. Since the beginning of the Project, the PolyOWC has been considered particularly interesting and promising, especially at the current technological stage, because:

- With respect to its traditional implementation (OWC with water or air turbine), it provides an evident simplification in design and architecture, by replacing the most complex component (the PTO itself), with a soft DEG unit, which represents the only moving part (at least for the case of fixed-structure OWC).
- As compared to other concepts (namely, the PolySurge and PolyBuoy [2]) that still derive from existing WEC architectures in which the traditional PTO unit has been replaced with a DEG, the PolyOWC does not require sophistications (e.g., the submerged articulated mechanism holding the DEG in PolySurge) and/or very complex and costly components (hinged submerged paddle, buoy interface and mooring). This maximizes the benefits brought by DEG application, which prompts this technology to be brought from the current research state to industrial development.
- With respect to direct-contact concepts with the membrane in direct touch with water [2], PolyOWC features lower complexity in terms of construction, practical operation, and control, and appears more suitable for short-term deployment of larger scale units.
- Due to its adaptability to different installation scenarios, PolyOWC enables an industrialization roadmap as follows: (1) first up-scaled installations will be on-shore OWCs so as to allow ease of monitoring and prevent typical drawbacks related to off-shore operations, and to enable further development of DEG technology; (2) successive development might foresee off-shore installations with larger OWC collectors fixed to platforms or other off-shore constructions; (3) the final stage of development will be off-shore moored arrays of OWCs, which would take advantage of large power and market scale.

In D4.1, three test campaigns have been reported: two on bottom-fixed PolyOWCs, and one on a moored PolyOWC. All of these devices were at a scale in the range of 1:50 and 1:40 with respect to hypothetic full-scale systems.

Owing to DEGs architectural simplicity, it has been possible to set-up experiments with fully-functional DEG PTO, yet at that small scale.

Experimental results were encouraging, as electric power outputs up to 0.9W (corresponding 360 MW at a scale 40 times larger) were produced.

In this report, we present results from the last two test campaigns, carried out on a larger scale PolyOWC prototype. The device, that features a scale of 1:25-1:30, has been tested at Flowave (Edinburgh) for 4 weeks in total (2 weeks in May 2016 and 2 weeks in September 2016).

The selected OWC collector architecture features axi-symmetric shape and is referred to as Poly-U-OWC. The U-OWC collector consists of two coaxial bodies: an inner body, which encloses the water column, and a coaxial outer cylinder. The cylindrical ring volume enclosed in between the two cylindrical bodies acts as an acceleration duct (namely, an added-mass duct), which has the aim of increasing the inertia of the system, thus making it possible to tune the device with incoming waves. Moreover, the presence of the external cylinder takes the water inlet section closer to the free surface, thus increasing the excitation force of the waves on the water column. Openings located at the bottom of the inner cylinder connect the added mass duct to the water column. In Figure 1 we show two schematic concepts of Poly-U-OWC. One device is bottom-fixed and is aimed to be installed in shallow water. The other one is floating (held in place by tension-leg moorings) and it is suitable to operate in offshore locations. In the picture, the DE PTO is implemented using several Circular Diaphragm DEGs (CD-DEGs) [3] per device to guarantee smaller size, ease of installation and replacement. In the experiments, however, a single DEG PTO has been used on the collector for simplicity of implementation.

With respect to previously tested concepts (e.g., bottom-based collectors tested in a wave flume), Poly-U-OWC better represents a potential full-scale architecture. In fact, its layout is adaptable to different

installation configurations (bottom fixed or moored), it can be tuned to different wave climates by properly adapting the collector dimensions, and it represents a potential candidate to progressively migrate the technology from near-shore installations to the off-shore market.

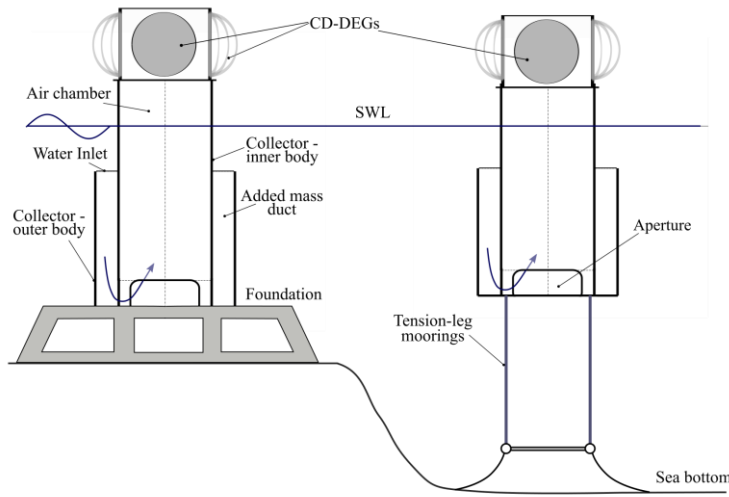


Figure 1. Impression of bottom-founded and moored U-OWCs with DEG PTO.

A description of the Poly-U-OWC prototype built for the tests can be found in Deliverable D3.3 [4], where details on the design procedure and dimensions choice are also provided. Photographs of the device in operation during the tests are shown in Figure 2.

With respect to previous tests, further scale up performed in the reported experiments represents a remarkable improvement from both the technological and scientific point of view, because:

- At the selected scale (1:25-1:30), consistent WEC power output is in the order of a few Watts. The DEG developed for this application is thus among the largest ever built, and represents one of the first efforts to migrate DEG technology from a small laboratory scale to a larger scale and a concrete application.
- Manufacturing of large DEGs like those employed in the reported tests (DEGs diameter was 39 cm) is challenging. The increased amount of DE material required for the target power output have made it necessary to realize DEGs with stacked multi-layered architecture.
- Differently from most WEC tank tests at this scale, where the PTO is only emulated by a break or damper, an electric power output has been successfully produced. Power outputs consistent with full-scale requirements have been measured (at the chosen prototype scale). Specifically, peak powers up to almost 4 W (i.e., 590 kW full-scale) have been produced.
- At this scale, validation of numerical models can take advantage of reduced hydrodynamic viscous losses. A complete validation of Poly-U-OWC sub-components models (collector hydrodynamics, DEG, etc.) has been possible.

A wide variety of tests have been carried out during the testing periods.

First, a characterization of the idle collector hydrodynamics (open collector, with water column free surface in contact with atmosphere) has been carried out and used to validate the collector hydrodynamic model. Upon installation of the DEG on the collector, a characterization of the system purely mechanical response (in absence of electric activation) has first been performed and used to validate coupled OWC-DEG models. Successively, electricity generation tests in different conditions (several mono and panchromatic sea states, different DEGs, different levels of DEG electric loading) have been carried out. Performance assessment of the device has been accomplished and a complete wave-to-wire model has been validated.

Survivability tests on the DEG PTO have also been carried out. In particular, the effect of apertures located on the OWC air chamber as a security measure in case of extreme seas has been assessed, and a validation of the OWC chamber model with relief valve has been performed.

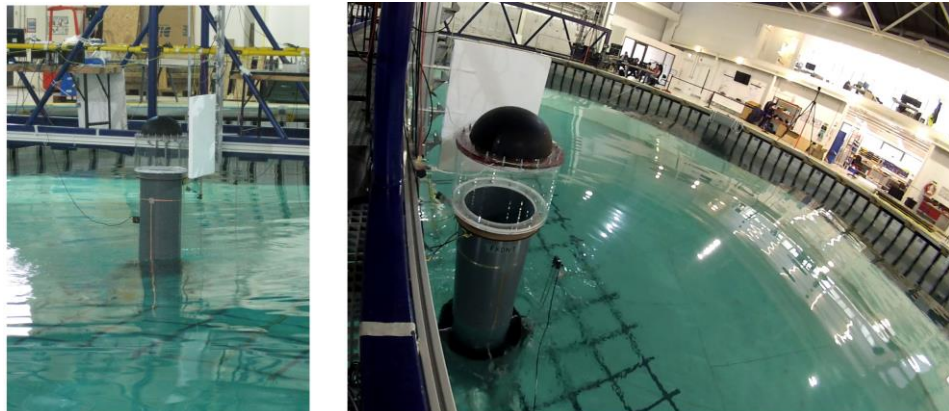


Figure 2. Shots of the U-OWC prototype operation with DE membrane during wave tank tests.

The contents of this report are organized as follows.

Sect. 2 provides a description of the experimental setup, of the power conditioning and measurement electronics, and of the testing procedures. A wide description of the U-OWC prototype, of design criteria, and of construction is also available in D3.3 [4].

Sect. 3 presents an analysis of experimental results. Results are sorted in the following categories: 1) hydrodynamic tests carried out on the open OWC collector without any DEG; 2) mechanical tests on the Poly-U-OWC, including U-OWC and CD-DEG, in absence of electric activation; 3) generation tests on fully-functional Poly-U-OWC with electric energy production; 4) survivability tests, similar to the mechanical Poly-U-OWC tests but with exceptional waves and eventual implementation of security measurements (e.g., aperture in the air chamber); 5) other tests, such as with combined waves and currents.

Sect. 4 presents validation of previously established models. Models validation follows an incremental approach. In particular, it starts from the validation of purely hydrodynamic collector model and adds different levels of complexity (DEG mechanical model, electric activation, etc.) at every step.

Finally, Sect. 5 draws the conclusions.

2. EXPERIMENTAL SETUP, PROCEDURE AND DATA PROCESSING

2.1 Prototype design

Design of the coupled WEC-DEG system has been carried out in accordance with the procedure introduced in Sect. 3 of D3.3 [4].

The following specifications have been taken into account: the device should feature a scale in the order of 1:30 and a target electric power output in the range of 2÷3 W (corresponding to 300-440 kW in full-scale).

At design level, a linearised model for both the hydrodynamics and the CD-DEG mechanical response has been used (the model is detailed in Sect. 3 of D3.3 [4]), and the frequency response of the system was examined, to match the WEC resonance with the target frequency (~ 0.5 Hz). The consistency of the chosen design with the target power output has been checked upon calculation of the cyclic convertible energy of the DEG (basing on operating constraints).

The choice of the device sizes has been carried out basing on the availability of commercial components to build the collector. Given the relatively large dimensions of the OWC at the target scale, commercial PVC piping has been employed for the construction.

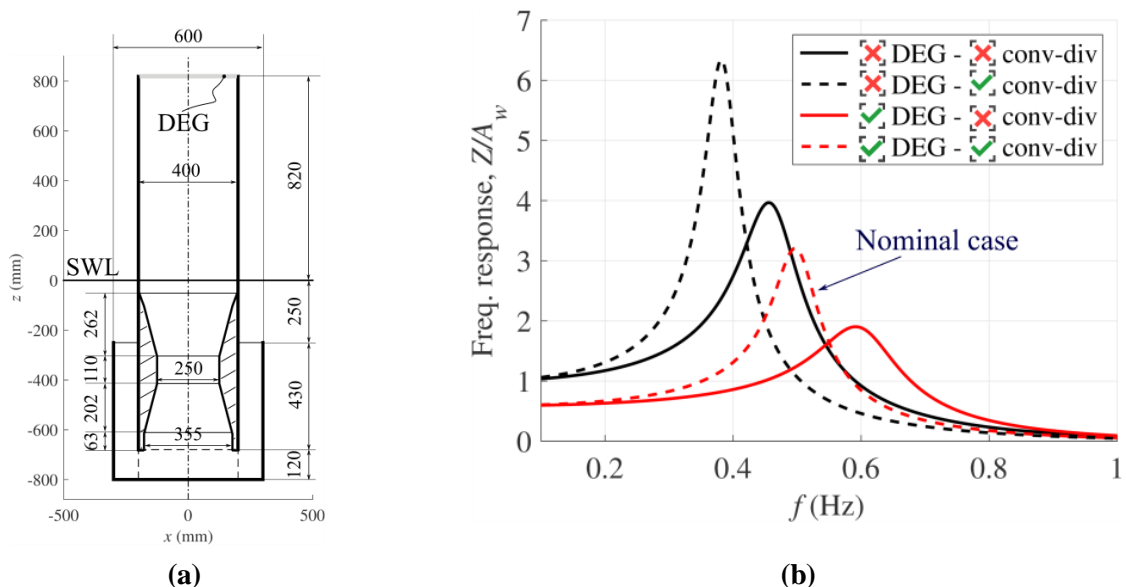


Figure 3. (a) Geometry and dimensions of the U-OWC prototype collector. (b) Frequency response of the U-OWC collector (with and without convergent-divergent duct), and of the system collector + DEG (with and without convergent-divergent duct).

Table 1. (a) VHB 4905 material properties. (b) Parameters of the nominal DEG PTO for U-OWC prototype.

Hyperelastic props (Mooney-Rivlin model)	$C_{10}=5.5$ kPa $C_{01}=0.57$ kPa
Rupture stretch, λ_u	9
Break-down electric field $E=E_0\lambda^{Re}$	$E_0=100$ MV/m $R_e=1$
Dielectric constant, ε	$4.2 \times 8.85 \times 10^{-12}$ F/m

(a)

Material	Acrylic VHB 4905
DEG stretched radius, e	195 mm
DEG unstretched thickness, t_0	2 mm
Pre-stretch, λ_p	3.75
Nr. Of in-parallel layers (DEG stack)	2

(b)

An appropriate design has been identified, which makes use of a piecewise linear convergent-divergent duct. The selected collector dimensions are in Figure 3.a.

Although the collector can house DEGs with different features, the nominal PTO is made of a commercial acrylic elastomer, namely VHB 4905 (by 3M), whose properties are listed in Table 1.a. As already explained in D4.1 [1] (see Sect. 3.3), although this material has large visco-elasticity and electric dissipation, and is not conceived for DE applications (it is an industrial tape), it is widely employed as DE in experiments as it is easy to handle, pre-stretch and stack in layers (thanks to its adhesiveness) [5], [6]. Moreover, its low rigidity makes it particularly suitable for small-scale experiments. The features of the nominal DEG PTO are given in Table 1.b.

The device is designed to house a single CD-DEG with diameter of about 400 mm, corresponding to 12 m at full-scale. The thickness in the flat pre-stretched configuration is 0.14 mm. As already discussed in D4.1 (Sect. 2) [1], the corresponding full-scale thickness is obtained by the small scale one multiplying by the square of the scale factor (i.e., the corresponding full-scale DEG thickness is 12.8 cm).

Although in the experiments a single DEG unit has been used, at full-scale the PTO is expected to be split in several smaller units, as shown in Figure 1.

The height of the air chamber (~0.8 m) has been chosen to facilitate operations from the tank gantry. Although a proper scaling of the air volume, which makes use of extended air chamber, has been discussed in D4.1 (Sect. 2.2) [1], no external air tank has been included in the setup reported here, to overcome technical issues related to pressure losses or dynamic effects in the piping.

Due to the mentioned aspects, the device should not be regarded as a prototype to scale up as it is. It rather represents a generic implementation of U-OWC with polymeric PTO, consistent with a 1:30 scale. Full-scale version is expected to slightly differ from prototype for DE material, collector design, and PTO layout.

Figure 3.b shows the amplitude of the water column oscillations (per unit of wave amplitude) as a function of frequency for different scenarios: open collector with no DEG (plain cylindrical inner collector section, or convergent divergent profile), and collector + DEG. Analysis of Figure 3.b shows the following:

- Oscillation amplitude in presence of DE membrane is smaller than open collector oscillations, due to the DEG stiffness.
- At low frequencies, the oscillation amplitude of the water column equals the wave amplitude if no DEG is present, otherwise it is lower (due to the membrane stiffness).
- The presence of the convergent-divergent duct increases the inertia of the water column, thus lowering the resonance frequency of the system and narrowing the resonance peak.
- Since this frequency response comes from linearization and neglects viscosity, oscillation amplitude is expected to be overestimated (especially at resonance).
- The figure shows that the presence of convergent-divergent duct provides a system that resonates at 0.5 Hz with a DE membrane.

2.2 Prototype construction

The prototype has been built combining commercial components (PVC piping for the collector cylinders and convergent-divergent duct) and custom-made cast acrylic parts (flanges, rings, connections).

The collector bodies have been made using PVC ventilation pipes, inserting 400 mm PVC pipe into 600 mm PVC pipe, securing it with 4 internal aluminum sectors.

The convergent-divergent duct has been realized using two PVC reductions for vent pipes. A wave gauge has been placed within the collector to measure the water column free surface elevation.

The bottom of the outer collector is an acrylic plate. A small gap has been left between the bottom plate and the outer cylinder to enable water draining as the device is taken out of the water. The inner pipe is placed 12 cm above the bottom plate to allow water passage (see Figure 3.a).

A manual valve has been put on the air chamber on the inner PVC pipe: the valve must be open as the device is sank, to keep pressure within the chamber at atmospheric value (otherwise the DEG would inflate), while it should be closed during operation.

The top part of the air chamber consists of a clear acrylic pipe, to allow visual inspection and filming of the membrane during downward deformation. The inner PVC pipe and the acrylic pipe are connected through acrylic flanges.

All of the connections (for instance glued joints) within the air chamber have been properly sealed to avoid air leaks.

The DEG assembly can be mounted on top of the air chamber acrylic pipe, clamped between two flanges (a lower one, attached to the acrylic tube, and a removable upper one).

A set of acrylic rings have been built to pre-stretch the membrane and mount it on the assembly. The rings have inner diameter, $2e = 390\text{mm}$, so as to be able to house DEGs with different thickness and pre-stretch but with fixed pre-stretched radius, e .

Further details on the collector components manufacturing and assembly can be found in D3.3 [4].

A photograph of the device installed on the Flowave tank floor (with floor fully up) is in Figure 4.a.

During tests, the device must be fixed to the tank floor, where threads are present. A gravity-based foundation has been built using Bosch profiles, which can be attached to the tank floor. The U-OWC collector is built upon this foundation structure (specifically, the collector bottom plate and outer cylinder are rigidly attached to the Bosch profiles).

Flowave tank has a movable floor, which is risen up (out of the water) to install/fix the device to the tank (see Figure 4.a), and is then lowered down to sink the prototype for operation. A picture of the sank device (floor down), prior to DEG installation, is in Figure 4.b. Maintenance operations, e.g., membrane installation and replacement, are carried out directly from the tank gantry (see Figure 4.c).

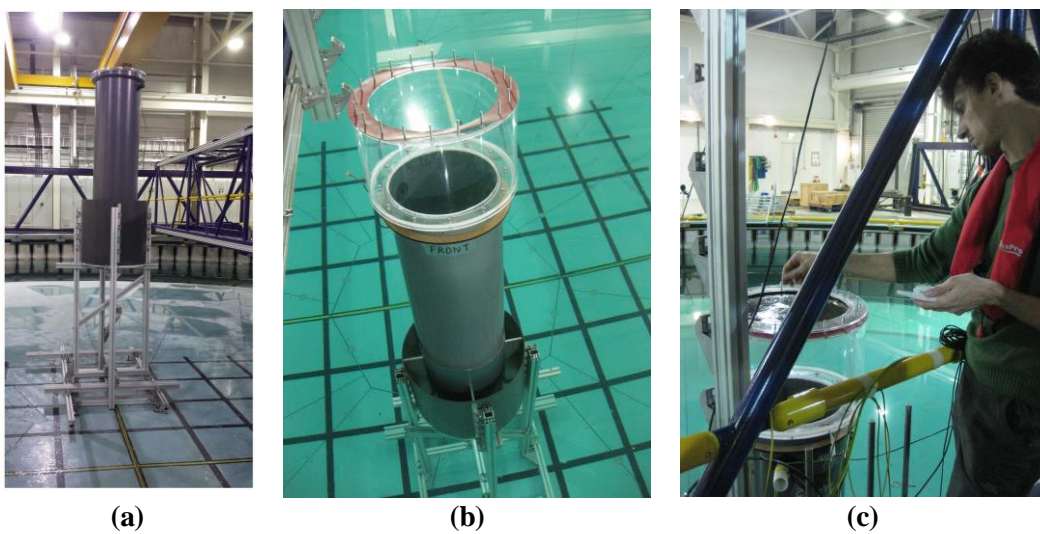


Figure 4. (a) Prototype assembly mounted on the tank floor. (b) Prototype installed in the tank (floor is fully down, and the device is sank). The picture shows the detail of the upper air chamber, made with a clear acrylic pipe (without DEG), on top of which a rubber sealing is present to lean the rings holding the DEG. (c) Shot of DEG installation on the collector from the gantry.

2.3 Control and electric layout

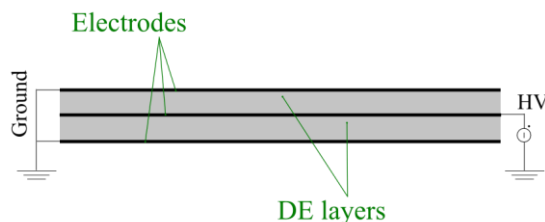
The prototype DEG PTO is a stack of two in-parallel DE layers and three electrodes (two on the stack outer faces, and one in between the two layers), in accordance with the layout defined in Figure 5.a. Outer electrodes are grounded, while High Voltage (HV) is applied on the central electrode, which is insulated from the environment for safety and to prevent charge dispersion in air. In the nominal design (see Table 1.b), each layer has unstretched thickness of 1 mm, and is obtained by bonding two VHB 4905 layers on top of each other. In the experiments, thicker layers have been also tested, up to a total DEG thickness $t_0 = 3\text{ mm}$ (1.5mm per layer).

Electrodes are made of conductive grease (MG-Chemicals 846), and they are connected to the wires of the circuit by means of a copper foil connecting the electrodes perimeter to the circuit terminals.

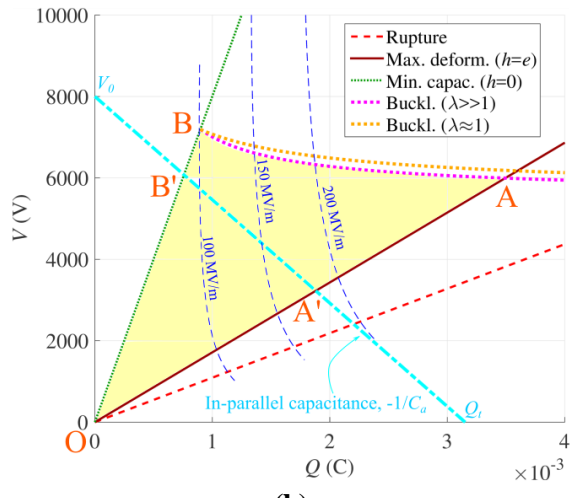
The feasible operating region of the DEG can be represented on a charge-voltage (Q - V) plane.

With reference to Figure 5.b, the Energy Conversion Cycle (ECC) featuring maximum-energy is bounded by the following curves:

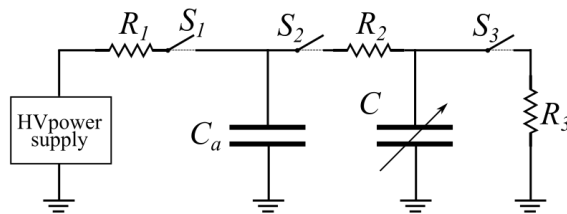
- OA: maximum capacitance curve. It has been assumed, here, that the maximum deformation of the membrane approximately coincides with the membrane hemispherical configuration (i.e., the membrane tip height, h , equals radius e).
- AB: buckling curve, i.e., the set of states in which the DEG is in a condition of marginal mechanical equilibrium at null stress.
- BO: minimum capacitance configuration, i.e. the flat equilibrium configuration (membrane tip displacement is null: $h=0$).



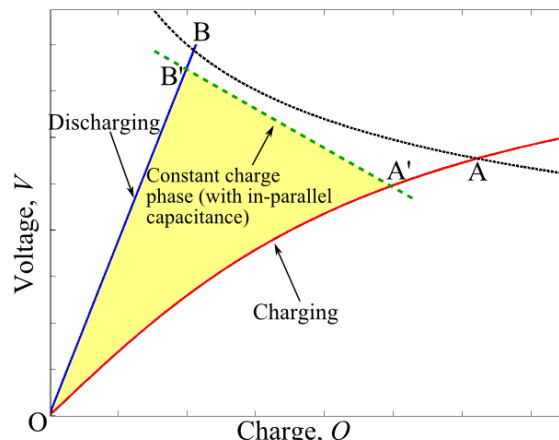
(a)



(b)



(c)



(d)

Figure 5. (a) Layout of the DE PTO (in the flat configuration). The DEG has two DE layers separated by an inner HV electrode. Ground electrodes coat the two outer faces of the DEG. (b) Nominal operating space with iso-electric-field lines highlighted, and practical ECC (OA'B'O) with in-parallel capacitance, C_a . (c) Power conditioning circuit of the DE PTO. (d) Example of real ECC (OA'B'O) on the Q - V plane: the charging curve (OA') is a bent-curve, corresponding to a constant position of the water column free surface.

The area enclosed by the cycle OABO is numerically equal to the maximum cyclic convertible energy. Assuming that, at the nominal frequency $f = 0.5$ Hz, the DEG is deformed by the wave up to the hemispherical configuration and the maximum energy cycle is performed (at a rate of two cycles per wave period, one upward and one downward), the resulting power would be ~ 9 W. This value is an upper limit for the convertible power, and it is not the actual expected power output of the prototype because

- Electric losses are not taken into account,
- The maximum energy cycle (OABO) is very difficult to implement in practice. Simplified sub-optimal charge-voltage paths are pursued using a simple conditioning circuit.

The electronic conditioning/measuring circuit layout for the experiments is shown in Figure 5.c. The circuit includes: 3 resistors (R_1 , R_2 , R_3), 3 HV switches, S_1 , S_2 , S_3 (HM12-1A69-150 by MEDER electronic), and 2 capacitors: the DEG (with variable capacitance, C) and an in-parallel capacitor with constant capacitance C_a . A HV power supply (10/10B-HS by TREK) is used to activate the DEG at each cycle. The power supply provides an output voltage of up to 10 kV.

The use of the in-parallel capacitance has been suggested in [7]. Such expedient makes it possible to approximate the maximum-energy cycle by simply performing energy harvesting cycles at constant total charge Q_t (with Q_t being the sum of the charges on the CD-DEG and on C_a). It can be easily demonstrated that, if the system is provided with a charge Q_t , which is kept constant during the useful electric activation phase, charge Q and voltage V on the CD-DEG electrodes vary accordingly to the following relationship:

$$V = C_a^{-1}(Q_t - Q). \quad (1)$$

Eq. (1) represents a straight line with slope $-1/C_a$ on the Q - V plane. In the example reported in Figure 5.b (where the DEG deforms up to $h = e$), this results in the ECC OA'B'O, where $C_a = 394$ nF and $Q_t = 3.15$ mC have been used. By properly choosing C_a and Q_t , the maximum-energy, cycle OA'B'O provides a good approximation of the maximum-energy cycle OABO.

During the tests, different values for C_a were used, depending on the DEG layout, ranging from $C_a = 247$ nF to $C_a = 394$ nF.

The adopted control strategy recalls that used in previous tests [1] and it is as follows: 1) the DEG is electrically activated when its capacitance reaches a maximum; 2) it is discharged when capacitance gets minimum; 3) is kept electrically inactive during rising capacitance phases. The different phases are triggered basing on relative pressure (and its derivative) measurements: when pressure is maximum/minimum, the DEG is maximally inflated upward/downward. When pressure is zero, the DEG is flat.

For the purpose of measuring the DEG capacitance at the instant of activation, capacitor C_a can also be used in the experiments to charge the DEG.

The sequence of operations composing the DEG control cycle is as follows:

- At the beginning of each cycle (while the DEG capacitance is rising), C_a is charged up to a fixed voltage V_0 (in Figure 5.b, $V_0 = 8$ kV) by the power supply.
- When the DEG capacitance reaches a maximum, S_1 is opened, S_2 is closed, and C_a reaches an equilibrium voltage, V_A , with C_{DEG} . By measuring the voltage drop on C_a , knowing its initial charge, it is possible to estimate the DEG capacitance, C_A , at the activation instant:

$$C_A = C_a \left(\frac{V_0}{V_A} - 1 \right) \quad (2)$$

- As the DEG capacitance decreases, S_2 remains closed and the charge on the parallel ($C_a + C$) is constant. By measuring the voltage V on the capacitors, it is thus possible to estimate the DEG capacitance variation.
- When the DEG is flat, S_2 is opened, S_3 is closed and the DEG is fully discharged on resistor R_3 . Switch S_3 is then opened and the successive cycle is started. DEG capacitance in the flat configuration is indicated by C_B , and V_B is the corresponding voltage on DEG and C_a .

To prevent membrane activation in the cycles where the membrane deformation is very small (especially in panchromatic waves), and energy generated would not even compensate the losses, a threshold on peak pressure is set: when pressure is maximum/minimum but pressure module is below the threshold, the DEG is not activated.

The energy harvesting controller is implemented on a real-time machine (Performance real-time target machine by SpeedGoat), running at a sample frequency of 10 kHz, via the Simulink Real-Time software environment.

Resistances R_1 and R_2 are needed respectively to smooth the HV power supply output (preventing oscillations induced by the supply dynamics), prevent current peaks and protect the switches.

A discussion on the choice of resistances values can be found in [4]. The resistance values can be taken within the following ranges: $R_1 \leq 170 \text{ k}\Omega$; $R_2 = 70 \div 150 \text{ k}\Omega$; $R_3 = 60 \div 300 \text{ k}\Omega$. Different combinations of resistance values (within the specified ranges) were used during the tests. The desired resistance values were obtained combining 50 $\text{k}\Omega$ HV resistors (SM204035002JE by Ohmite).

2.3.1 Generated power measurement

Energy generated by the DEG at each cycle can be measured indirectly.

The employed procedure relies on instant voltage measurement on DEG and C_a . Differently from previous tests [1], where energy was calculated by estimating the DEG capacitance from DEG tip height, h , here DEG capacitance at activation (C_A) is measured from charge conservation using Eq. (2) (although V_0 is prescribed, it is measured with the HV probe on C_a for better accuracy) and capacitance C_B at the discharging instant (when the DEG is flat) that is constant and known (from direct measurement on the flat DEG stack).

The electric energy generated by the DEG in a cycle is:

$$W_e = \frac{1}{2} C_B V_B^2 - \frac{1}{2} C_A V_A^2 + \frac{1}{2} C_a (V_B^2 - V_A^2) \quad (3)$$

where V_A and V_B are measured with HV probes.

W_e is the sum of three terms, with the following meaning. The first term is the energy recovered from the DEG at discharging. The second (negative) term is the energy supplied to the DEG at activation. The third term accounts for the energy generated by the DEG and transferred to C_a .

Two objections to this procedure might be done, as discussed in the following.

In this estimate, it has been assumed that DEG capacitance remains constant during charging and discharging phases. However, in [1], it has been observed that the DEG capacitance varies during the charging phase.

In particular, with reference to Figure 5.d, the generic ECC is represented by cycle OA'B'O: during charging phase, the water column free surface position is approximately constant (because charging is approximately instantaneous), therefore voltage application provokes a jump in membrane shape (and capacitance) and in air pressure. The various points of curve OA' are equilibrium points for the membrane at intermediate voltages. This effect is not present during instant discharging (curve B'O is a straight line), because in the flat configuration voltage does not influence the mechanical equilibrium.

Prior to run generation tests on the prototype, the shape of charging curves (like OA' in Figure 5.d) has been characterized experimentally, using the circuit in Figure 5.c. The air chamber of the OWC has been pressurized. Capacitance C_a has been charged and then connected in parallel to the DEG (by closing S2): the equilibrium voltage has been measured, and the corresponding DEG capacitance has been estimated from charge conservation. The measurement has been repeated over a set of charging voltages of C_a and at different pressurizations of the air chamber. This has allowed to map the charging curves. These have shown that if one computes the cyclic generated energy fitting a constant value of C_A in Eq. (3) (rather than considering the real shape of the charging curve) the overestimate in the cyclic generated energy (W_e) is less than 1% in the most energetic cycles. For this reason, constant C_A and Eq. (3) have been used in the calculation of W_e for simplicity.

The second objection is that connecting C_a in parallel to the DEG (at the beginning of each ECC) provokes dissipation of a consistent amount of energy stored in C_a . E.g., if one connects two capacitors in parallel (one charged and the other discharged), 50 % of the energy stored in the charged capacitor gets dissipated, regardless the resistance in the circuit. However, this expedient is only used to indirectly measure DEG capacitance. The amount of energy dissipated during DEG charging is not kept into account in the computation, which only accounts for the actual amount of electric energy converted by the DEG.

3 DATA PROCESSING AND RESULTS

In this section, details on experimental data post-processing is performed, and results from different classes of tests are presented. The aim of these experimental tests was:

- Provide evidence of Poly-U-OWC operating principle demonstrating that: 1) it achieves resonance within the predicted frequency range; 2) its capability of producing electric power in both regular and irregular waves; 3) the effectiveness of security measures (relief valve) in extreme sea states.
- Validate established numerical models against acquired measurements. This task is detailed in Sect. 4.

For each test, the wave tank was started from a calm (fully flat) condition. To guarantee the achievement of the desired sea-state condition, a waiting time of about two minutes was respected prior to begin data acquisition.

The considered values of wave frequency (peak frequency, if panchromatic waves) range from 0.3 Hz to 0.7 Hz (corresponding to wave periods of 8-18 s at a scale 30 times larger), while wave height (significant height for panchromatic waves) ranges from 0.1 m to 0.25 m (3-7.5 m at full-scale).

Besides varying the wave conditions, different tests have been carried out varying the following parameters: 1) DEG layout (pre-stretch, thickness t_0); 2) in-parallel capacitance C_a (see Figure 5.c); 3) level of electric load, i.e., charging voltage V_0 of the in-parallel capacitor (see Figure 5.b).

Relevant variables have been acquired as follows:

- Undisturbed wave elevation in the device far-field, and water column elevation are measured with resistive wave-gauges by Edinburgh Designs. Wave gauge measurements are acquired at 64 Hz using a custom driver (by Edinburgh Designs) and National Instrument acquisition system available at Flowave.
- Air chamber gauge pressure was measured with a piezo-resistive sensor (MPX12 by Freescale Semiconductor). Voltages on DEG, in-parallel capacitor and power supply output (when electric activation is present), measured with custom made high-impedance ($10 \text{ G}\Omega$) probes. All of these signals have been acquired at 10 kHz using the same real-time target machine used to control the DEG. Signals post-processing includes pressure measurements filtering with a median filter of order 100, and probes signals smoothing with a moving average filter with a span of 100 samples.
- Membrane deformed shape was monitored through a high-speed camera (Point Grey GS3-U3-23S6M-C with lens 250F6C, using acquisition software FlyCapture 2.9). A white board was attached to the U-OWC collector behind the membrane, to enhance the contrast of the membrane shape with the background. An example of video frame from high-speed camera acquisition is shown in Figure 6. Pictures were acquired at 100 fps. Image post-processing has been carried out using computer-vision techniques, described in D4.1 (Sect. 5.2) [1]. The output of the video identification procedure is time-series of membrane tip elevation, $h(t)$.

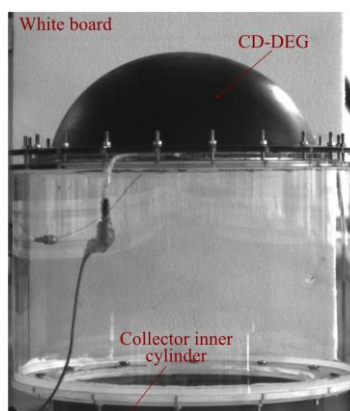


Figure 6. Video frame from high-speed camera acquisition

A selection of results is presented in the following. Results are sorted in the following categories: 1) hydrodynamic tests, with fully-open collector and no CD-DEG; 2) mechanical tests with idle CD-DEG, in

absence of electric activation; 3) electricity generation tests; 4) survivability tests; 5) mixed wave and current tests.

Particular attention is set on electricity generation tests, while the other classes of tests are discussed more in detailed in Sect. 4 with regards to models validation. Generation tests are particularly interesting not only from the point of view of WEC assessment (being among the few small-scale tank tests with fully-functional electro-mechanical PTO), but also because they feature one of the largest DEGs ever tested.

3.1 Hydrodynamic tests (fully open collector)

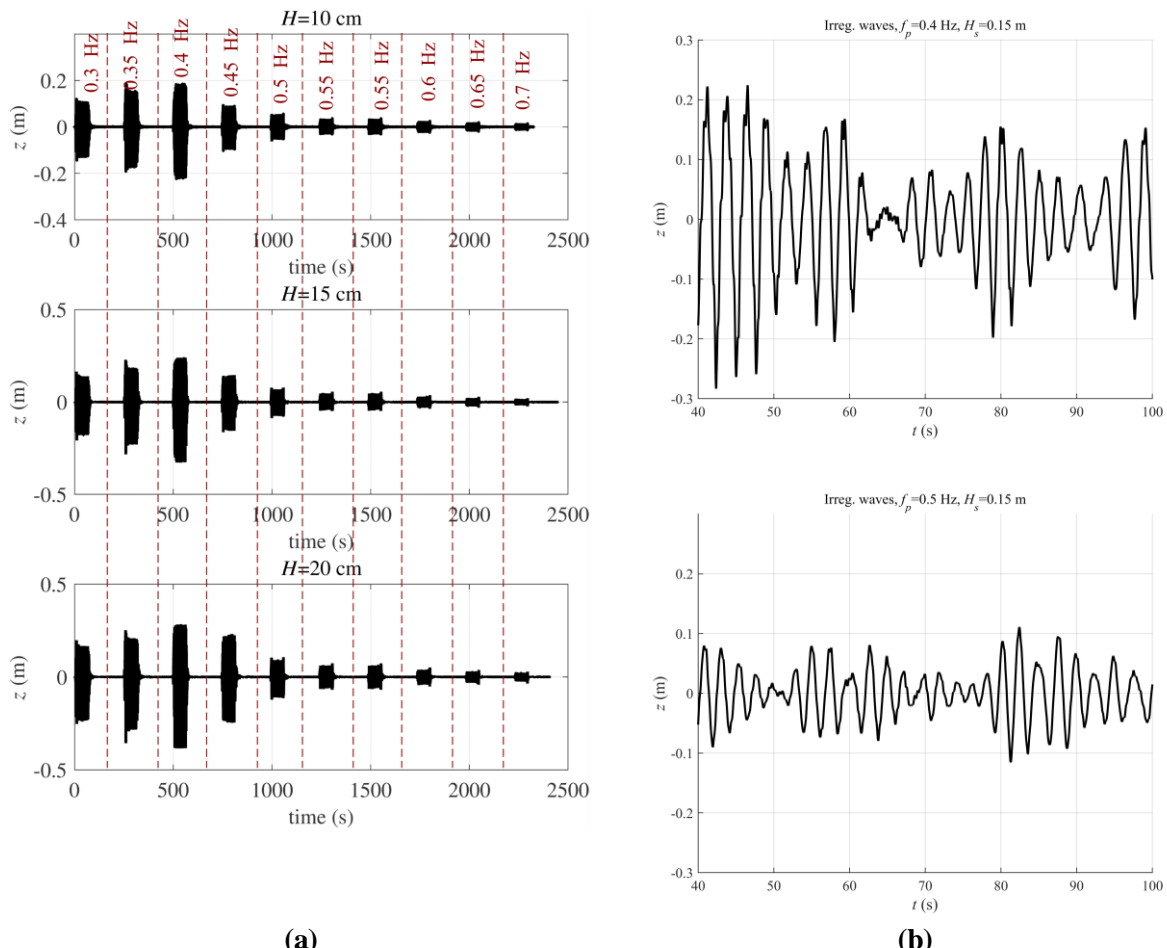


Figure 7. Water column displacement (z) time-series for hydrodynamic tests on fully-open collector. (a)

Monochromatic tests. Each dataset features constant wave height, while frequency is varied throughout the different time windows. (b) Time-series relative to two panchromatic tests. Irregular waves were generated using Jonswap spectrum with peak factor $\gamma=3.3$.

A set of tests aimed at characterizing the hydrodynamic response of the collector were performed. The objective of these tests were to identify the resonance frequency of the water column (in absence of the membrane), and providing benchmark data for hydrodynamic model validation.

Hydrodynamic tests were run both in regular and irregular waves.

Three sets of regular wave tests were done: in each test, a constant wave height (H) was used, and a sweep in frequency was performed: 9 different frequencies, from 0.3 to 0.7 Hz (spaced apart by 0.05 Hz) were considered. A waiting time between two consecutive frequencies was introduced, to restore a calm (fully flat) condition in the tank. Water column elevation (z), measured by the inner wave gauge (within the collector) is reported in Figure 7.a for the three monochromatic datasets. Water column oscillation amplitude variation throughout the different frequencies provides clear insight into the collector frequency response. In particular, resonance of the open collector is at approximately 0.4 Hz. Variation in oscillation

amplitude passing from $H = 0.1$ m to $H = 0.15$ m is larger than from $H = 0.15$ m to $H = 0.20$ m, i.e., a saturation in oscillation amplitude occurs at larger wave heights, due to dissipation and non-linearity (e.g., the geometric non-linearity introduced by the convergent-divergent duct).

Example of water column elevation time-series in irregular waves are in Figure 7.b. Panchromatic waves were generated using Jonswap spectrum and peak enhancement factor (γ) of 3.3.

Again, at peak frequencies closer to the resonance frequency, oscillation amplitude is larger. The position of the resonance peak is consistent with the prediction provided by Figure 3.b (black dash-dot line).

3.2 Mechanical tests with idle CD-DEG

In the following we present relevant time-series obtained by purely mechanical tests (no electric activation) on the Poly-U-OWC prototype housing a CD-DEG membrane (with the features shown in Table 1.b). A comparison of the device response with and without the DE membrane is presented.

With reference to regular waves featuring the same amplitude and different wave periods, Figure 8 shows relevant time-series for the case with open collector (no membrane) and with idle (electrically inactive) nominal DEG installed. In the first case, only the water column elevation z inside the collector is shown (red dashed line), while for the second case air gauge pressure, Δp and membrane tip displacement, h are also of interest. Corresponding z time-series (with and without DEG) are translated with respect to each other in order to align them (for easier comparison).

Comparison of the plots shows that:

- In the case with idle DE membrane, oscillations are largest at the intermediate frequency of $f = 0.5$ Hz, that is, indeed, the design resonance frequency;
- Free surface oscillation in absence of membrane are largest at the lowest frequency, as observed before. This demonstrates that the presence of the DEG moves resonance peak at larger frequencies.
- As expected, when the collector resonates without DE membrane, free surface oscillations are larger than those of the resonating collector+DEG system (at 0.5 Hz).
- time-series of z , Δp , and h are substantially in-phase, i.e., the DEG has quasi-static response, and its dynamics is negligible with respect to that of the water column.

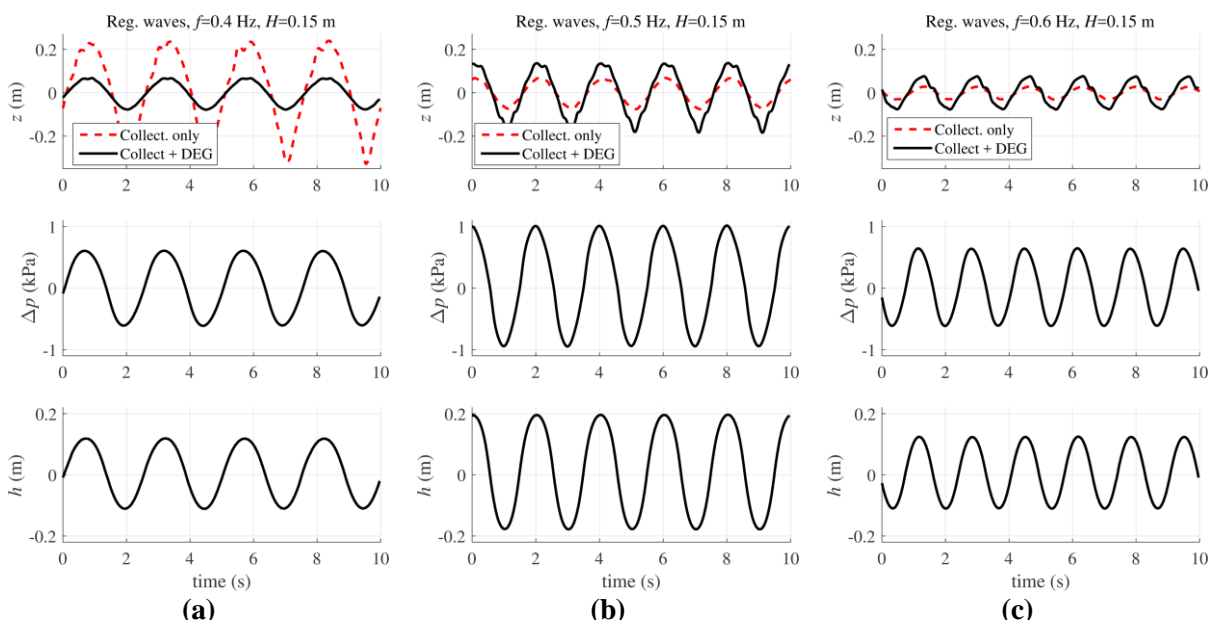


Figure 8. Experimental time-series of water column displacement (z), air chamber gauge pressure (Δp), and membrane tip elevation (h) for three different regular wave tests. The tests feature same wave height ($H=0.15$ m) and different wave frequencies: (a) $f = 0.4$ Hz, (b) $f = 0.5$ Hz, (c) $f = 0.6$ Hz. Water column displacement is compared with that of the open collector (no DEG) in presence of the same sea states.

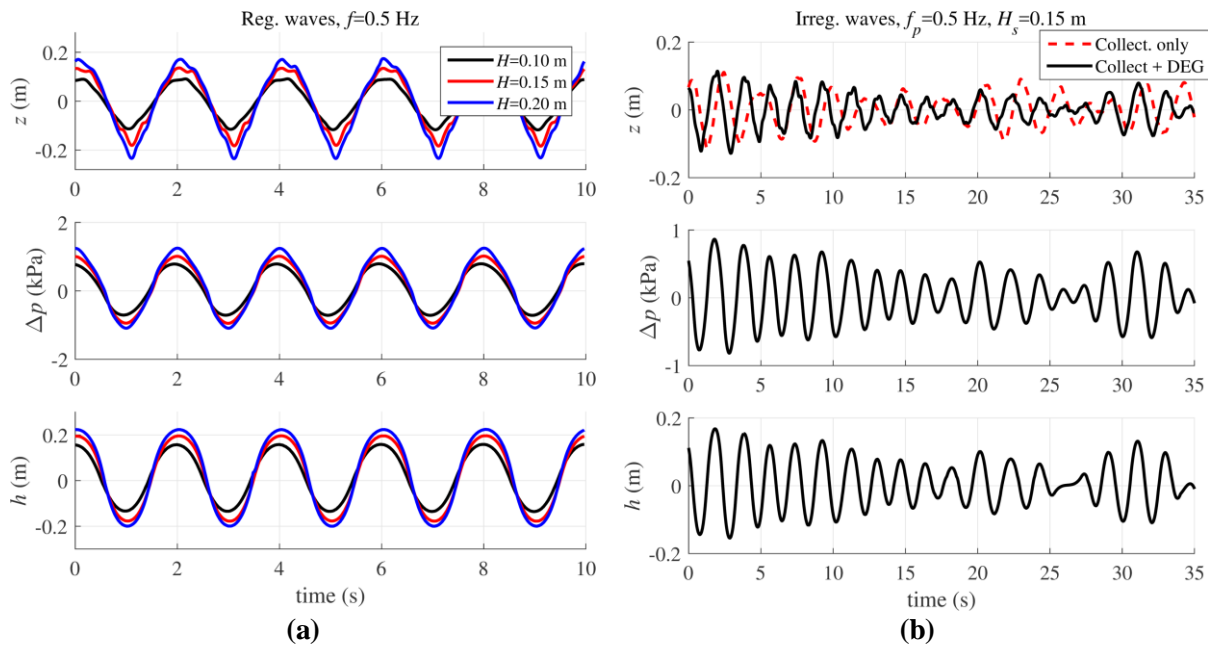


Figure 9. Experimental time-series of water column displacement (z), air chamber gauge pressure (Δp), and membrane tip elevation (h) in two scenarios: (a) Different monochromatic sea states with same frequency ($f = 0.5$ Hz) and different wave heights ($H = 0.10, 0.15$ and 0.20 m). (b) Panchromatic wave with peak frequency $f_p = 0.5$ Hz, significant wave height, $H_s = 0.15$ m (Jonswap spectrum, $\gamma = 3.3$). In the latter case, water column oscillation, z , is compared with that of the open collector (no DEG).

Figure 9.a shows the effect of wave amplitude on the system response. Time-series refer to monochromatic waves with $f = 0.5$ Hz and to the case with nominal DEG installed. Different time-series sets are translated with respect to each other in order to align them. The plot shows that oscillation amplitudes have greater increase when H varies from 10 cm to 15 cm than when it varies from 15 cm to 20 cm. This is an effect of non-linear DEG behavior, which results in a saturation of deformation and displacements as excitation forces increase.

Examples of irregular wave time-series are in Figure 9.b. The upper sub-plot shows the water column elevation in presence of nominal DEG (black solid line) compared with that of the open U-OWC collector (red dashed lines). Such time-series refer to the same incoming wave. The phases of the two signals are not corrected, i.e., incoming waves are in-phase, and phase difference between black and red line are a result of different frequency response owing to the membrane presence. For the case with DEG PTO, gauge air pressure and tip elevation are also shown.

3.3 Electric generation tests results

In this section, an evaluation of the U-OWC prototype in terms of electricity generation is performed. Relevant time-series are shown both for regular and irregular waves tests, and generated power in different scenarios is calculated.

With reference to a DEG PTO with initial thickness $t_0 = 2$ mm, pre-stretch $\lambda_p = 3.39$, composed by two in-parallel layers, and to monochromatic sea states with $H = 0.15$ m and different frequency, we compare relevant time-series before and after electric activation (Figure 10). Plots refer to experiment with in-parallel capacitance $C_a = 394$ nF and charging voltage on the in-parallel capacitor $V_0 = 6000$ V.

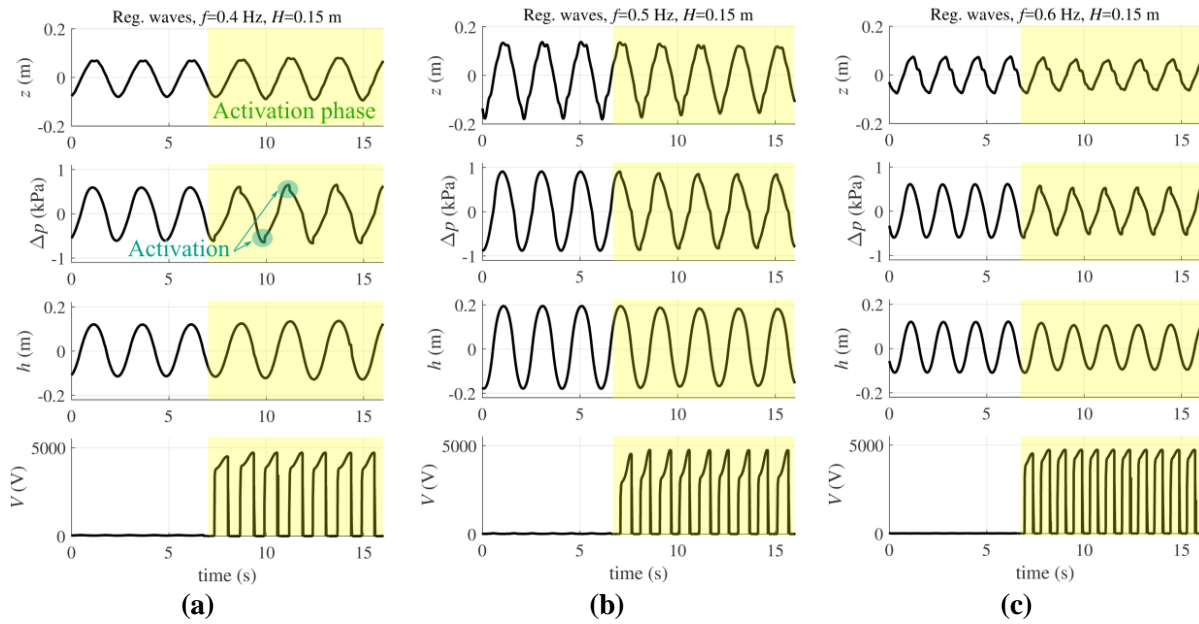


Figure 10. Experimental time-series of water column displacement (z), air chamber gauge pressure (Δp), membrane tip elevation (h) and DEG voltage (V) for three regular sea states. The tests feature same wave height ($H = 0.15$ m) and different wave frequencies: (a) $f = 0.4$ Hz, (b) $f = 0.5$ Hz, (c) $f = 0.6$ Hz. Phases during which the controller is active are shadowed in yellow. In the first picture, the effect of instant activation (provoking a pressure drop) is highlighted.

From Figure 10, we observe the following:

- Consistently with the control strategy described in Sect. 2.3, the DEG is activated when its capacitance is maximum and kept active while its capacitance decreases, i.e., voltage on DEG + C_a rises during active generation phases. DEG charging is nearly instantaneous.
- Oscillation amplitude of z , Δp and h changes before and after activation. Numerical comparison of the oscillation amplitudes shows that oscillation amplitude in presence of activation is lower for $f = 0.5$ and 0.6 Hz, while it is larger at 0.4 Hz. Electric activation has two effects on the WEC dynamics: 1) it damps the WEC oscillation, as it subtracts mechanical energy to the system; 2) it makes DEG rigidity decrease, as electrostatic stress subtracts to elastic stress, thus shifting the resonance peak at lower frequency. The system natural frequency (basing on purely mechanical response) is about 0.5 Hz. When the DEG is activated, oscillation amplitude at excitation frequencies $f \geq 0.5$ Hz decreases, both because the system is damped and natural frequency decreases. At 0.4 Hz, the shift in resonance peak overcomes the increase in damping, and oscillation amplitude slightly increases.
- As observed in previous tests and explained in D4.1 [1] (Sect. 5.1), quick electric activation provokes a jump in air pressure and membrane tip position. Experimental Δp time-series clearly shows this effect. The jump in h is not easily visible from the time-series, both because it is small (due to high air rigidity at small scale, small variations in volume provide visible pressure variations) and because of the accuracy of the graphical identification procedure for the measurement of DEG tip deflection.

Figure 11 shows the same set of time-series for a panchromatic wave case. The DEG has nominal features (Table 1.b), capacitance C_a is 394 nF, and $V_0 = 5000$ V. In the plots, time-series in absence and in presence of electric activation are compared (red dashed and black solid lines respectively). From the plot, the difference between pressure profiles in idle and active case, due to instant DEG activation (inducing a jump in pressure), is clearly visible. Voltage profile shows that the membrane is not activated when oscillations are small (i.e., pressure absolute value below 10 Pa).

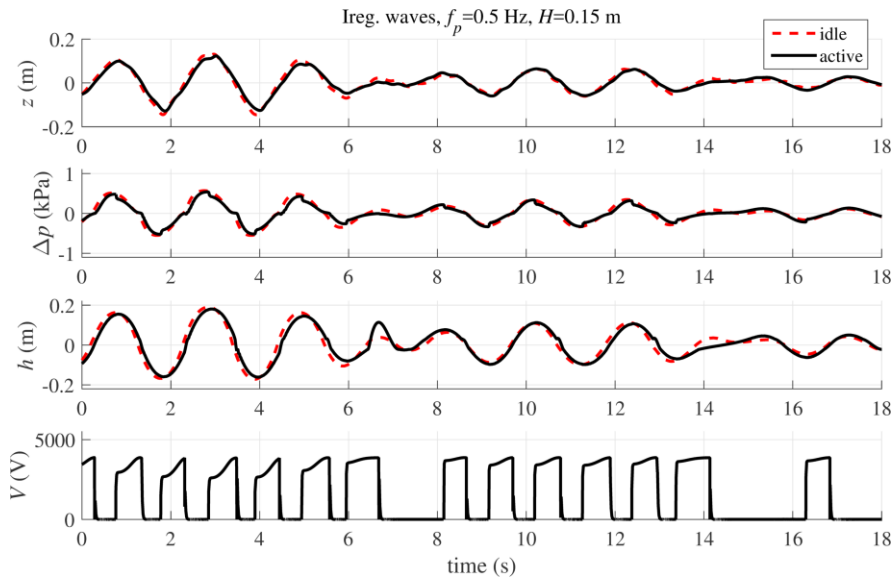


Figure 11. Experimental time-series of water column displacement (z), air chamber gauge pressure (Δp), membrane tip elevation (h) and DEG voltage (V) for an irregular sea state featuring Jonswap spectrum with $\gamma = 3.3$, $H_s = 0.15$ m, $f_p = 0.5$ Hz. Red dashed lines refer to the case with idle DEG, while black solid lines are with functioning controller.

3.3.1 Regular waves performance assessment

In this section, we resume performance results obtained in a variety of tests with different membranes, different values of in-parallel capacitance and supply voltage V_0 , and different monochromatic sea states. Results are presented in terms of DEG electric power output, P_u . P_u is computed from cyclic converted energy, W_e , computed according to Eq. (3), and from the wave frequency f_w . Considering that the DEG performs two ECCs per period, the following equality holds: $P_u = 2W_e f_w$.

In Figure 12 we report the produced electrical power from different sets of experiments (either featuring different DEG architectures, with unstretched thickness of 2 or 3 mm, or different in-parallel capacitance and supply voltage). In each set, the membrane power is computed over a range of sea states.

Power in the plots, is computed from the average of W_e over the different cycles. The first cycle after activation has been removed from the analysis as it generally features different DEG oscillation amplitude with respect to the steady state response.

Plots show the following:

- Power output is maximum at the natural frequency of 0.5 Hz (i.e., the natural frequency of the inactive system).
- Although the power available from the waves increases with the square of the wave height, electric power output rises less than quadratically with H , due to progressive saturation in DEG deformation.
- Electric peak power surpasses 2 W in the case with 2mm-thick DEG, and 3 W in the case with 3mm-thick DEG, corresponding to 300 and 440 kW respectively at full-scale. This result is extremely encouraging from a wave energy application perspective, considering that it has been obtained with a non-optimal and rather dissipative material. It is expected that with purposely developed DE materials, performance would be further enhanced. Besides, with regards to the DEG itself, this result is one-of-a-kind, as to date DEGs at this scale have been scarcely investigated, especially in combination with an application of practical interest like renewable energy harvesting.

Beside the results presented here, other tests have been performed. A few experiments with a DEG and an electric layout equal to that employed in the tests of Figure 12.c have been done, using a higher electric load (namely $V_0 = 8000$ and 8250 V). The maximum generated power was registered during those tests. In Figure 13, we report DEG and in-parallel capacitor voltage time-series for a couple of tests with $H = 0.25$ m, $f_w = 0.5$ Hz, and $V_0 = 8000$ and 8250 V respectively. The resulting average power output (steady-state) was 3.58 W (530 kW full-scale equivalent) in the first case and 3.80 W (560 kW full-scale equivalent) in the second case, with peak powers of 3.69 and 3.93 W during the first cycle.

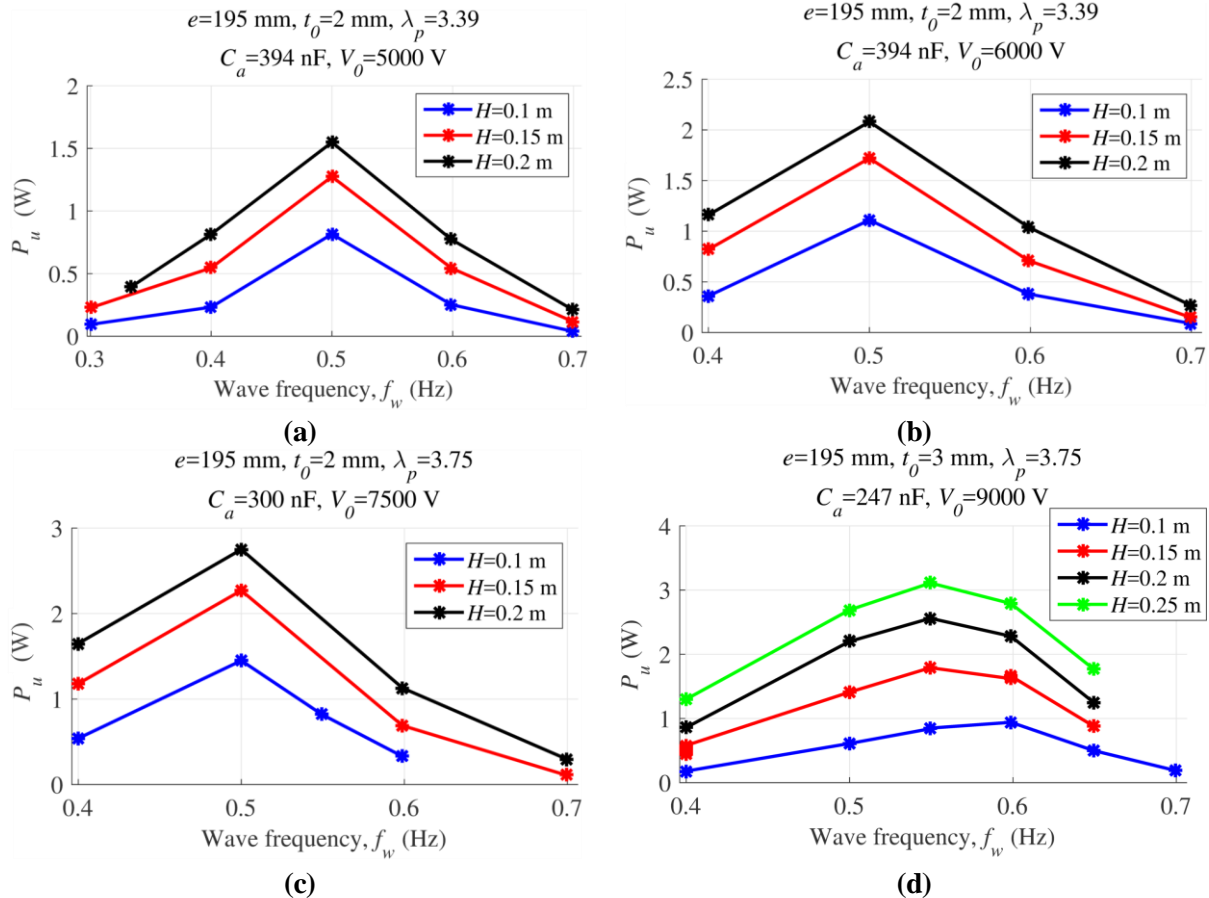


Figure 12. Experimental electric power output of the U-OWC in the different sea conditions. Plots refer to the following combinations of parameters: (a) $t_0 = 2 \text{ mm}$, $\lambda_p = 3.39$, $C_a = 394 \text{ nF}$, $V_0 = 5 \text{ kV}$ (b) $t_0 = 2 \text{ mm}$, $\lambda_p = 3.39$, $C_a = 394 \text{ nF}$, $V_0 = 6 \text{ kV}$, (c) $t_0 = 2 \text{ mm}$, $\lambda_p = 3.75$, $C_a = 300 \text{ nF}$, $V_0 = 7.5 \text{ kV}$, (d) $t_0 = 3 \text{ mm}$, $\lambda_p = 3.75$, $C_a = 247 \text{ nF}$, $V_0 = 9 \text{ kV}$.

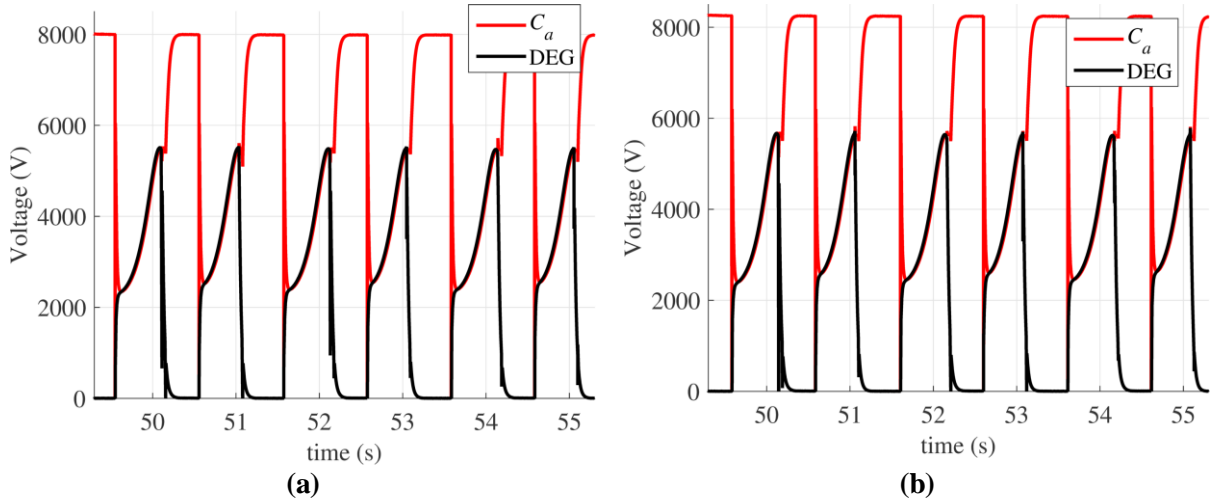


Figure 13. Time-series of voltage on C_a and on the DEG for the two tests that featured maximum generated power. The parameters used in the tests are: $e = 195 \text{ mm}$, $t_0 = 2 \text{ mm}$, $\lambda_p = 3.75$, $C_a = 300 \text{ nF}$, and (a) $V_0 = 8 \text{ kV}$, (b) $V_0 = 8.25 \text{ kV}$ respectively.

3.3.2 Irregular waves performance assessment

In this section, we report results of electric power output P_u in a selection of panchromatic wave tests. In the tests, irregular waves were generated using a Jonswap spectral distribution.

With respect to regular waves experiments, a less detailed analysis has been performed (in terms of number of tests and sea states resolution). The aim of irregular wave tests was to assess the effectiveness of the controller in irregular waves rather than providing a full characterization of power output performance.

Differently from monochromatic tests, the mean power P_u in a given sea state is here computed as the sum of the electric energy generated in the different cycles divided by the time duration of the generation phase.

For each sea state, an instant power is also defined. The instant power is piece-wise constant and it is defined as the ratio of the energy generated in a certain cycle divided by the duration of that cycle, identified by two successive apertures of switch S_2 (see Figure 5.c).

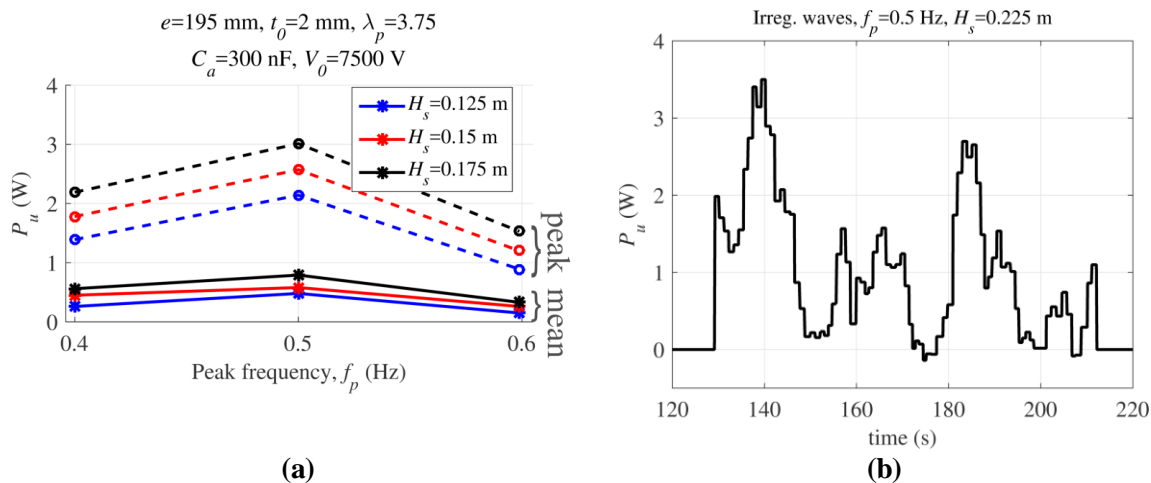


Figure 14. (a) Experimental electric power output of the U-OWC in the different panchromatic sea conditions (Jonswap spectrum with $\gamma = 3.3$). The plot refers to the following combination of parameters: $t_0 = 2\text{mm}$, $\lambda_p = 3.75$, $C_a = 300 \text{ nF}$, $V_0 = 7.5 \text{ kV}$. (b) Instant power time-series for a panchromatic sea state featuring $f_p = 0.5 \text{ Hz}$ and $H_s = 0.225 \text{ m}$. The membrane features are the same of Fig. (a).

In Figure 14.a we report the produced electrical power from a set of experiments with different panchromatic sea states. In the figure, solid lines represent average power (over the experiment) for the different sea states, while dashed lines stand for the peak instant power. As for the monochromatic cases, power is maximum at $f_p = 0.5 \text{ Hz}$, although the dependence of power (especially mean power) on frequency is weaker than in monochromatic waves. Mean power up to 1 W was generated, with peaks up to 3 W. Besides the tests described in Figure 14.a, other tests were carried out using the same membrane asset. In particular, Figure 14.b shows the instant power time-series for a panchromatic wave with $f_p = 0.5 \text{ Hz}$ and $H_s = 0.225 \text{ m}$, for which a mean power of 1.1 W and a peak power of 3.5 W were measured. The time-series shows that

- The power is zero over certain time intervals, i.e., the membrane is not activated in those instants because oscillations are too small;
- The controller is effective also in panchromatic waves. In particular, with the chosen threshold values for activation, power output is positive practically all the time (there are no dissipative cycles).

In Figure 15, we compare mean power outputs of a CD-DEG operated in irregular waves featuring $H_s = 0.15 \text{ m}$ and $f_p = 0.5 \text{ Hz}$ (i.e., the monochromatic peak power frequency) and different values of Jonswap γ parameter. Mean power output increases with γ (i.e., when the spectrum becomes more “peaky”). In fact, in this case, increasing γ leads the prototype closer to resonant monochromatic operation.

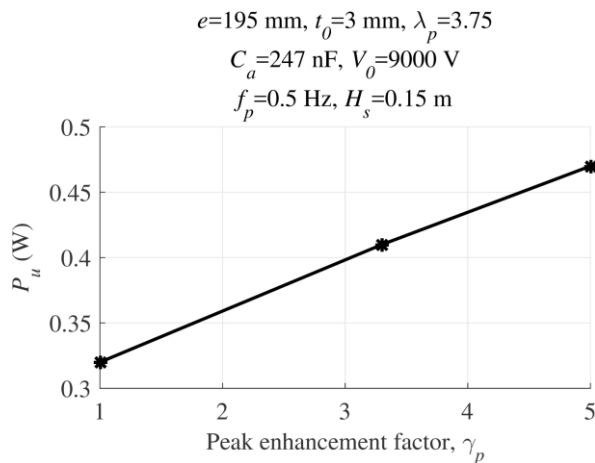


Figure 15. Experimental mean power output of the U-OWC in panchromatic sea states featuring Jonswap spectrum with $f_p = 0.5$ Hz and $H_s = 0.225$ m, and different values of the peak enhancement parameter, γ . The plot refers to the following combination of parameters: $t_0 = 3$ mm, $\lambda_p = 3.75$, $C_a = 247$ nF, $V_0 = 9$ kV.

3.4 Survivability tests

Survivability tests have been carried out to assess the effectiveness of valves on the OWC air chamber as a security measure to protect the CD-DEG in case of extreme seas. These tests have been run in absence of electric activation, for it is supposed that in exceptional sea conditions the DEG would be kept idle in safety mode.

In practical application, it is expected that overpressure inception in the Poly-OWC air chamber would be prevented by means of relief valves, which allow air flow passage only when gauge pressure surpasses a certain threshold.

For simplicity, survivability tests have been carried out by opening a set of apertures on the prototype air chamber, and keeping them open throughout the whole set of survivability tests.

A manual valve (see Figure 16.a) is present on the prototype by design. The valve is normally used to keep air pressure at atmospheric value as the device is sank (see Sect. 2.2). The valve has been kept closed during regular operation, while it has been opened to perform a first class of survivability tests. The manual valve consists in a circular aperture of 35 mm diameter, which can be manually closed with a plug.

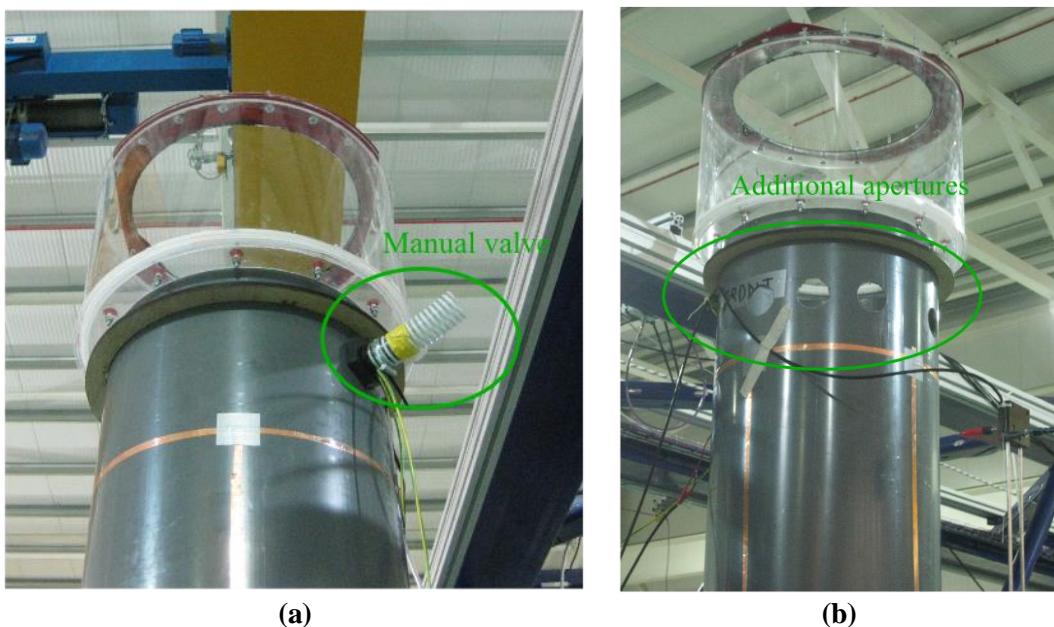


Figure 16. (a) Detail of the manual valve used during tank shut-down/start-up and for survivability tests. (b) Detail of additional apertures cut on the collector side at the end of the test session, to assess the effect of increasing aperture section on the DEG deformation.

In Figure 17.a we report relevant time-series (water column displacement, air pressure, DEG tip displacement) relative to a regular sea state for the two cases with closed air chamber and open air chamber (i.e., manual valve open). In the plots, wave frequency is 0.5 Hz. Plots demonstrate that the valve is responsible for a reduction in air pressure and DEG deformation. Water column displacement is also reduced, because the aperture provokes a variation of the mechanical stiffness of the system DEG+air, thus shifting the resonance of the device.

To assess the influence of increasingly large apertures on the DEG deformation damping, at the end of the test sessions, a set of circular apertures (each one with a diameter of 52 mm) have been cut on the emerged part of the collector (see Figure 16.a). In Figure 17.b we report relevant time-series in an extreme monochromatic sea state featuring $H=40$ cm (corresponding to 12 m at full-scale) and $f_w=0.5$ Hz, with an increasing number of open apertures on the air chamber (manual valve is closed).

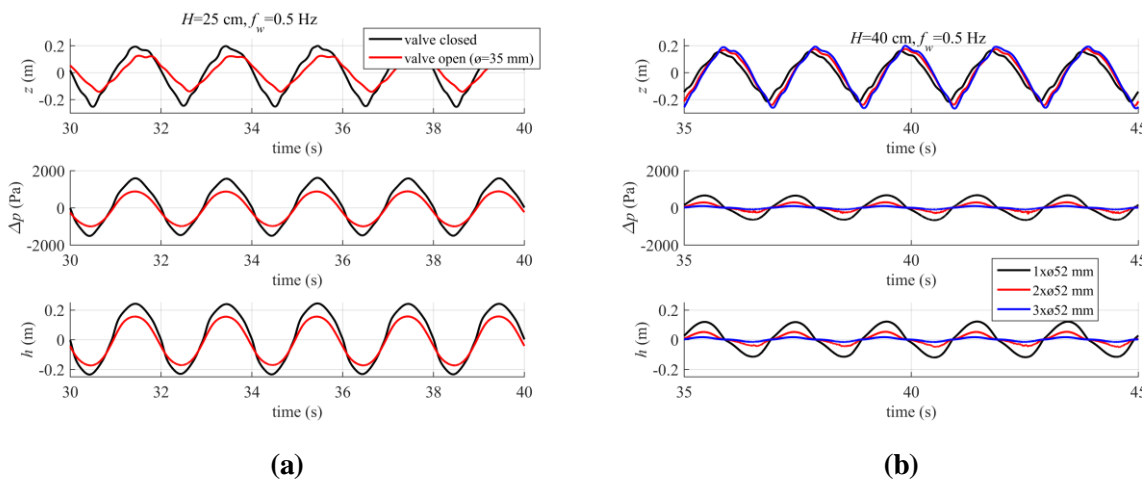


Figure 17. (a) Comparison of water column surface, air gauge pressure, and tip displacement in a regular wave with 0.5 Hz frequency and 25 mm height, in two cases: closed air chamber (regular operation), manual valve open (depowered safety mode). (b) Tests with increasing number of apertures (52 mm diameter each) on the air chamber. Comparison of relevant time-series in an extreme wave with 0.5 Hz frequency and 40 cm height.

By increasing the number of apertures, water column oscillation in the chamber undergoes minor variations, while pressure and membrane deformation rapidly fall to zero. This proves the effectiveness of valves as a security measure. Water column oscillation modification owes to variations in the frequency response of the system (the apertures modify the stiffness perceived by the water column), while membrane and pressure damp down due to increasing air flows through the apertures.

3.5 Tests with waves and currents

A set of mechanical tests with combined waves and currents have been carried out on the Poly-U-OWC prototype, to assess the effect of dynamics modification induced by currents.

As the prototype is bottom-fixed, it was expected a priori that no significant modifications would have been induced by the currents but the well-known wave height modifications [8]. Furthermore, effect of combined wave & current loads on foundations survivability is clearly not assessable from these tests, as the prototype foundation is not representative of a full-scale foundation.

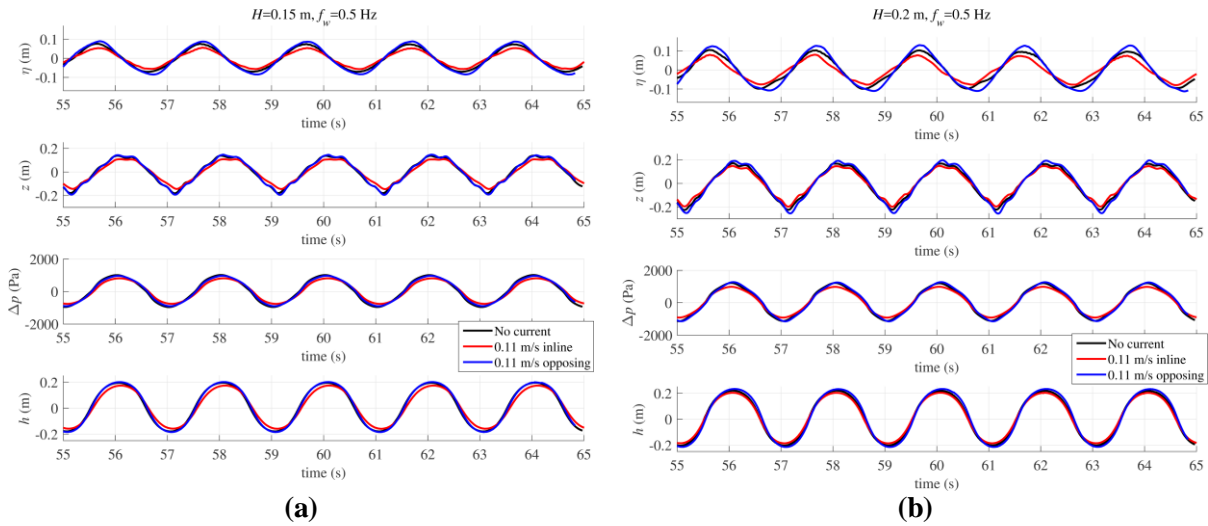


Figure 18. Comparison of relevant variables time-series (undisturbed wave elevation, water column displacement, gauge pressure, membrane tip) in absence of current (only waves), with inline waves and currents, and with current opposing waves. The two plots are for two regular commanded sea states: (a) $H = 0.15 \text{ m}$, $f_w = 0.5 \text{ Hz}$, (b) $H = 0.20 \text{ m}$, $f_w = 0.5 \text{ Hz}$.

In Figure 18, we compare relevant time-series (relative to two different monochromatic waves) for the cases with waves only, waves + inline current of 0.11 m/s (i.e., waves propagation direction is the same of current direction), and opposing waves and currents.

As expected, no relevant differences are observed in the device dynamics, but small modifications in oscillation amplitudes due to current-induced wave amplitude modification. In particular, wave amplitude decreases (with respect to the commanded value) when current has the same direction of waves, and increases if current is in the opposite direction. Wave height modifications can be seen from the top subplots in Figure 18 (where we show the undisturbed wave elevation in the device far-field), and they reflect also on the other time-series (water column oscillation, air pressure, membrane deformation).

4. MODELS VALIDATION

In this section we address mathematical models validation against experimental results. Established wave-to-wire models are the combination of several mathematical sub-models (hydrodynamic sub-model, DEG mechanical model, electrical model) and a proper calibration of uncertain parameters, which require to evaluate the validity of the single sub-models beforehand of that of the wave-to-wire model as a whole. For this reason, validation is approached by incremental steps, starting from the validation of the collector hydrodynamics and introducing different levels of complexity (DEG elastic model, DEG activation, valve model) at each step.

4.1 Poly-U-OWC mathematical model

In this section, Poly-U-OWC model is recalled. Descriptions of the model are also given in D5.4 [9] and D3.4 **Error! Reference source not found.**. With respect to the models detailed in those documents, here a more detailed hydrodynamic model has been used, which keeps into account the hydrodynamic non-linearity introduced by the convergent-divergent duct within the collector.

Models description is divided in the following sub-models: hydrodynamic model (i.e., collector model), CD-DEG model, air chamber model (closed air chamber, or air chamber with open security valve).

4.1.1 Collector hydrodynamic model

We make reference to the U-OWC collector shown in Figure 19. We assumed that the OWC collector does not move (it is fixed or kept in place by proper moorings), thus the only degree of freedom is the water column free surface displacement. We consider a reference ζ - η - ζ frame with vertical ζ axis and the origin lying on the Still Water Level (SWL). The OWC features:

- An inner chamber housing the water column itself. The water elevation in this chamber with respect to the SWL is z . The cross section radius of the inner chamber is indicated with $r(\zeta)$, as it generally varies with ζ . In correspondence of the water column free surface, $\zeta = z$ and $r(\zeta) = r(z)$.
- A horizontal inlet section (with the shape of a circular ring), located at $\zeta = \zeta_i$, through which water enters/leaves the collector.
- An acceleration duct (collector outer body), that drives water from the inlet section to the main collector body. The duct has outer diameter D_o and inner diameter D_i .

Water velocity in the various horizontal cross sections of the device is assumed uniform and perpendicular to the cross-sections. We thus assume that the transversal component of the velocity (lying on the cross-section plane) is much lower than the axial component, because the slope of the collector walls with respect to the vertical is mild.

The water velocity in a generic cross section of the main chamber is indicated with $v(\zeta)$ ($v(\zeta) = \dot{z}$ at the free surface), and it is positive if the water column level is rising. The constant velocity within the added-mass duct is indicated by v_i . Due to water incompressibility and mass conservation, the following equalities hold for any value of ζ :

$$\dot{m} = \rho_w \pi r^2(\zeta) v(\zeta) = \rho_w \pi (D_o^2 - D_i^2)/4v_i = \rho_w \pi r^2(z) \dot{z} \quad (4)$$

where \dot{m} is the water mass flow through the inlet section (positive if entering the collector).

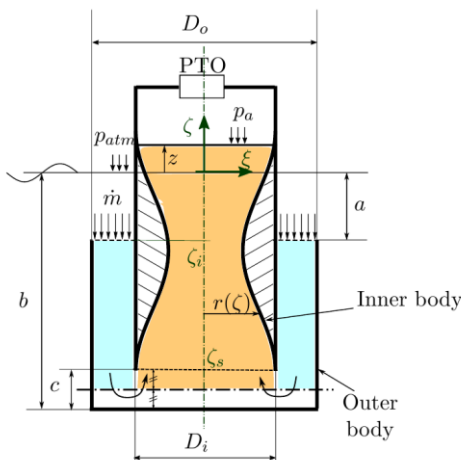


Figure 19. Definition of U-OWC dimensions and control volume

Since in the passage from acceleration duct to main chamber the water flow bends and reverts its direction, it is assumed that a stagnation volume exists at the basis of the collector, where the water can be assumed still. The stagnation surface lies at $\zeta = \zeta_s$ and, in Figure 19, it is marked with dash-dot line below which water is considered still. We assume that the stagnation surface lies exactly halfway along the aperture that separates the device bottom from the inner cylinder (i.e., the aperture that connects inner and outer bodies).

In this analysis, we describe the water column dynamics through coordinate z , and derive the equations of motion from an energy balance on the control volume housed in the collector above the stagnation line. Such a volume is bounded by the stagnation line, the OWC lateral walls, the water inlet section, and the water column free surface, and it is indicated by shadowed surfaces in Figure 19.

The global energy balance for the reference control volume is as follows:

$$\dot{E}_k + \dot{E}_g = \dot{W}_v + \dot{W}_a + \dot{W}_{in} \quad (5)$$

where

- E_k is the kinetic energy of water within the control volume and it reads as follows:

$$E_k = \frac{\rho_w}{2} \left(b - a - \frac{c}{2} \right) v_i^2 + \int_{-b+c/2}^z \frac{\pi \rho_w r^2(\zeta) v(\zeta)}{2} d\zeta = \pi \rho_w r^4(z) \left(4 \frac{b-a-\frac{c}{2}}{D_0^2 - D_i^2} + \int_{-b+c/2}^z \frac{d\zeta}{r^2(\zeta)} \right) \dot{z}^2 \quad (6)$$

- E_g is the potential gravitational energy of water within the control volume. Using the stagnation line as set point for potential energy (i.e., potential energy is zero on that plane), E_g reads as:

$$E_g = E_{g,i} + \pi \rho_w g \int_{-b+\frac{c}{2}}^z r^2(\zeta) \left(b - \frac{c}{2} + \zeta \right) d\zeta \quad (7)$$

where $E_{g,i}$ is a constant and it stands for the potential energy of the (constant) water volume comprised in the acceleration duct, while the second addendum is the potential energy of the water within the collector inner body.

- \dot{W}_v is the power dissipated by the hydrodynamic viscous forces. We define the viscous loss coefficient, $K_{v,i}$, with reference to the dynamic pressure at the inlet section, thus we obtain:

$$\dot{W}_v = -\dot{m} \frac{K_{v,i}}{2} v_i |v_i| = -\frac{8\pi\rho_w K_{v,i} r^6(\zeta)}{\left(D_o^2 - D_i^2\right)^2} \dot{z}^2 |\dot{z}| \quad (8)$$

where $K_{v,i}$ is a viscous coefficient (usually in the order of magnitude of unity).

- \dot{W}_a is the power associated to the mechanical work done by air (in the OWC air chamber) on the free surface:

$$\dot{W}_a = -\pi r^2(z) p_a \dot{z} \quad (9)$$

where p_a is the absolute pressure in the air chamber.

- \dot{W}_{in} is the power entering the system through the inlet section. It is composed by the following addenda: atmospheric pressure + hydrostatic pressure insisting on the inlet section, wave induced pressure on the surface, p_w , kinetic and potential energy density of the water flowing through the inlet section:

$$\begin{aligned} \dot{W}_{in} &= \dot{m} \left[\frac{p_{atm} + \rho_w g a}{\rho_w} + \frac{p_w}{\rho_w} + \frac{v_i^2}{2} + g \left(b - a - \frac{c}{2} \right) \right] \\ &= \pi r^2(z) \dot{z} \left[p_{atm} + p_e + p_r + \frac{8r^4(z)}{(D_o^2 - D_i^2)^2} \dot{z}^2 + \rho_w g \left(b - \frac{c}{2} \right) \right] \end{aligned} \quad (10)$$

where p_w has been split into two addenda: one owing to wave excitation force (p_e), the other owing to radiated waves (p_r).

Rearranging equations (5)-(10), the following dynamic equation is obtained:

$$M_z(z)\ddot{z} = -C_{\dot{z}^2}\dot{z}^2 - \pi\rho_w gr^2(z)z - 8\pi\rho_w K_{v,i} \frac{r^6(z)}{(D_v^2 - D_i^2)^2} |\dot{z}|\dot{z} + \pi(p_e + p_r - \Delta p)r^2(z) \quad (11)$$

where the following definitions have been introduced:

- $M_z(z)$ is the generalised inertia of the control volume (reduced to coordinate z):
 -
 - $$M_z(z) = \pi \rho_w r^4(z) \left(4 \frac{b-a-\frac{c}{2}}{D_o^2 - D_t^2} + \int_{-b+\frac{c}{2}}^z \frac{d\zeta}{r^2(\zeta)} \right) \quad (12)$$
 - $C_{\dot{z}^2}$ is the coefficient (depending on z) of the quadratic term owing to non-linear inertia and mass advection:

$$C_{\dot{z}^2} = 2\pi\rho_w r^2(z) \left\{ \left[4 \frac{b-a}{D_o^2 - D_i^2} + \int_{-b+\frac{c}{2}}^z \frac{d\zeta}{r^2(\zeta)} \right] r(z)r'(z) + \frac{1}{4} - \frac{4r^4(z)}{(D_o^2 - D_i^2)^2} \right\} \quad (13)$$

where $r'(z)$ stands for the first derivative of $r(z)$.

- $\Delta p = p_a - p_{atm}$ is air gauge pressure.

In practical applications, it is expected that the U-OWC collector would be much smaller than the wavelength, i.e., the device is conceived to operate as a point absorber. The excitation force can be thus approximated by the Froude-Krylov contribution only neglecting the diffraction component, as stated in [10]. By fitting the expression of an undisturbed linear wave (regular wave with height H and frequency ω) into equation (11), the excitation force reads as follows:

$$F_e = \pi p_e r^2(z) = \frac{\pi r^2(z) \rho_w g H}{2} \mathcal{L} \frac{\cosh(k_w(h_w-a))}{\cosh(k_w h_w)} \cos(\omega \tau) \quad (14)$$

where k_w is the wave number, h_w the water depth, and time is denoted by τ and factor \mathcal{L} comes from an integration on the inlet section and reads as follows:

$$\mathcal{L} = \frac{16}{\pi(D_o^2 - D_i^2)} \int_0^{\pi/2} \int_{D_i/2}^{D_o/2} \xi \cos(k_w \xi \cos \theta) d\xi d\theta \quad (15)$$

From this equation, an expression for the non-linear wave excitation coefficient as a function of z , is found:

$$\Gamma_z(\omega, z) = \pi r^2(z) \rho_w g \mathcal{L} \frac{\cosh(k_w(h_w-a))}{\cosh(k_w h_w)}. \quad (16)$$

Radiated wave load, $F_r = \pi r^2(z) p_r$, is more difficult to compute, as the radiation potential is a function of z and \dot{z} and it is not known a priori. It is then convenient, at least for this contribution, to make use of the linear formulation. We hereby assume that the radiation force can be written as follows:

$$F_r = -M_\infty \ddot{z} - \int_0^\tau k(\tau - \xi) \dot{z}(\xi) d\xi \quad (17)$$

where M_∞ is the infinite frequency-added mass. In the presented formulation, the inertia of the water column in the collector has been already kept into account through $M_z(z)$, while M_∞ is a further inertial contribution that adds up to $M_z(z)$. In the U-OWC, it is expected that the dominant inertial contribution owes to the displacement of the fluid within the collector, thus $M_z(z) \gg M_\infty$. We than assume that $M_\infty = 0$.

The convolution kernel, k , has the following well-known frequency-domain expression:

$$K(\omega) = -\omega^2(M_{ad}(\omega) - M_\infty) + i\omega B_r(\omega) \quad (18)$$

where $M_{ad}(\omega) - M_\infty$ is the frequency-dependent component of the added mass and $B_r(\omega)$ is the radiation damping.

Owing to the device axial-symmetry, the radiation damping can be computed using Haskind relation:

$$B_r(\omega) = \frac{\omega k_w \Gamma_z^2(\omega, 0)}{2\rho_w g^2 \Upsilon}, \quad \text{with} \quad \Upsilon = \left[1 + \frac{2k_w h_w}{\sinh(2k_w h_w)} \right] \tanh(kh_w) \quad (19)$$

The frequency-dependent component of the added mass can be promptly computed using Kramers-Kronig relation:

$$M_{ad}(\omega) - M_\infty = -\frac{2}{\pi} \int_0^\infty \frac{B_r(\xi)}{\omega^2 - \xi^2} d\xi \quad (20)$$

In numerical simulations, the convolution integral in equation (17) can be approximated with a linear state-space model.

4.1.2 DEG electro-mechanical model

CD-DEG model has been abundantly described in D1.2 [12] and D4.1 [1]. Here, with reference to the reduced model introduced in those references, we recall the fundamental assumptions and equations.

A schematic of the CD-DEG in the undeformed configuration and deformed inflated configuration is in Figure 20.

The model uses the following assumptions:

- the CD-DEG deforms as a spherical shell with tip height h (positive for upward deformation) and radius R ,
- the shell deformation is equibiaxial (i.e., $\lambda_1 = \lambda_2$) all over the DEG,
- from the electrical point of view, the CD-DEG can be considered as a deformable parallel-plate capacitor with non-uniform thickness.

Assuming that the CD-DEG response is quasi-static, the equations describing the DEG response are the following:

$$\begin{aligned} \Delta p &= \frac{4h}{h^2 + e^2} \frac{t_0}{\lambda^2} \sigma \\ \lambda &= \lambda_1 = \lambda_2 = \lambda_3^{-2} = \frac{h^2 + e^2}{ee_0} \\ \sigma &= \lambda \left. \frac{\partial \Psi(\lambda_1, \lambda_2)}{\partial \lambda_1} \right|_{\lambda_1 = \lambda_2 = \lambda} - \varepsilon E^2 \end{aligned} \quad (21)$$

where Δp is the air gauge pressure, h is the membrane tip displacement (positive upward), t_0 and e_0 are the undeformed membrane thickness and radius respectively, λ and σ are equibiaxial stretch and stress at the membrane tip, E is the applied electric field, ε is the DE dielectric constant, ψ is the hyperelastic strain-energy function [10], whose expression depends on a constitutive model.

The electric field E at the DEG tip relates to the voltage V as follows:

$$E = \frac{\lambda^2 n_L V}{t_0} \quad (22)$$

where n_L is the number of DE layers in the DEG stack, which equals 2 in the presented experiments. The following hyperelastic model (namely, Mooney-Rivlin model [13]) has been assumed:

$$\psi(\lambda_1, \lambda_2) = A_h (\lambda_1^2 + \lambda_2^2 + \lambda_1^{-2} \lambda_2^{-2} - 3) + B_h (\lambda_1^{-2} + \lambda_2^{-2} + \lambda_1^2 \lambda_2^2 - 3) \quad (23)$$

where A_h and B_h are constitutive parameters.

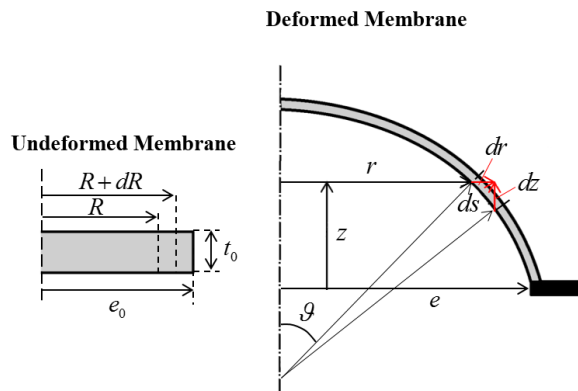


Figure 20. Circular CD-DEG in undeformed (left) and deformed (right) configuration

As regards the capacitance of the CD-DEG, its expression is

$$C(h) = \frac{\pi \varepsilon e^2}{3t} \left[\left(\frac{h^2 + e^2}{e^2} \right)^3 + \left(\frac{h^2 + e^2}{e^2} \right)^2 + \left(\frac{h^2 + e^2}{e^2} \right) \right], \quad (24)$$

where $t = t_0 \lambda_p^{-2}$ is the membrane thickness in the flat configuration, and $\lambda_p = e/e_0$ is the pre-stretch.

It is worth remembering that equations (21)-(24) hold under the assumption that the CD-DEG deformation is prevalently equibiaxial and the deformed shape is a spherical shell, i.e., the air volume subtended by the membrane is function of h as follows:

$$\Omega_c = \frac{\pi}{6} h (h^2 + 3e^2). \quad (25)$$

4.1.3 Air chamber model

In regular conditions, it is assumed that the closed air volume, Ω_a , evolves in an adiabatic way. Assuming that in the equilibrium configuration the membrane is flat ($\Omega_c = 0$) and pressure is atmospheric, the following equation applies:

$$p_a \Omega_a^\gamma = p_{atm} \Omega_{a,0}^\gamma, \quad (26)$$

where $\gamma = 1.4$ is the air adiabatic ratio, and the air volume Ω_a in a generic configuration relates to the equilibrium air volume, $\Omega_{a,0}$, as follows:

$$\Omega_a = \Omega_{a,0} - \int_0^z \pi r^2(\zeta) d\zeta + \Omega_c, \quad (27)$$

In rough sea conditions, the relief valve is open and the air chamber is open towards atmosphere. The thermodynamics of OWC air chamber is described in [14]. Neglecting the kinetic energy of the air flowing through the valve and assuming that the inlet/outlet air stream has the same density, ρ_a , and temperature, T_a , of the air in the chamber (see equation (5) in [14]), the following equations hold, which are the mass conservation, the energy balance (considering the system adiabatic) and the ideal gas law respectively:

$$\frac{d}{dt} (\rho_a \Omega_a) + \rho_a \dot{Q} = 0 \quad (28)$$

$$\frac{R_g}{\gamma-1} \frac{d}{d\tau} (\rho_a \Omega_a T_a) = -p_a \dot{\Omega}_a - \frac{\gamma R_g}{\gamma-1} \rho_a \dot{Q} T_a \quad (29)$$

$$p_a = R_g \rho_a T_a \quad (30)$$

where R_g is the specific gas constant and \dot{Q} is the air volume flow rate through the orifice (positive if air exits).

The previous set of equations lead to the following equation for the dynamics of the air chamber:

$$\Delta \dot{p} = -\frac{\gamma(\Delta p + p_{atm})}{\Omega_a} (\dot{\Omega}_a + \dot{Q}). \quad (31)$$

The equation of the air volume flow rate, \dot{Q} , through the valve orifice has the following well-known form:

$$\dot{Q} = \text{sign}(\Delta p) \frac{C_v A_v}{\sqrt{1 - \left(\frac{A_v}{A_{ref}}\right)^2}} \left(\frac{2|\Delta p|}{\rho_a} \right)^{1/2}, \quad (32)$$

where A_v is the valve aperture section, A_{ref} is a reference transversal section of the OWC (e.g., the section in correspondence of which the valve is located, which has inner diameter of 490 mm), and C_v is the coefficient of discharge, known either from calibration or from technical tables.

Combining Eq. (31) with Eqs. (27) and (32) provides a coupling between OWC dynamics, DEG model and air dynamics.

4.2 Model validation

Validation is carried out following an incremental approach, i.e., starting from the validation of purely hydrodynamic collector model, and increasing levels of complexity (DEG mechanical model, electric activation, etc.) at every step.

Mathematical models discussed in this section rely on the formulation presented in Sect. 4.1. The equations of the model are implemented in a Matlab & Simulink environment. Specifically, a Simulink block diagram has been created, and separate blocks have been written for the different sub-models (hydrodynamics, air chamber, DEG response, control).

Results have demonstrated that the model is very efficient in predicting the different phenomena involved in the U-OWC operation and the effect of mutual interaction among sub-systems (OWC collector, DEG membrane, controller). A good accuracy in the estimate of relevant variables quantitative trend has been also achieved.

4.2.1 Hydrodynamic model validation

Non-linear hydrodynamic model of the U-OWC collector (including a convergent-divergent duct in the collector inner body) is described in Sect. 4.1.1. The model relies on the calculation of a number of parameters, namely, non-linear excitation coefficient $\Gamma_z(\omega, z)$, and linear radiation parameters (calculated using Haskind and Kramers-Kronig equations). The radiation convolution is approximated with a state-space model.

The collector hydrodynamic model is validated against monochromatic tests results on open collector (with no membrane, and water column free surface contacting atmosphere), i.e., using the water column displacement, z , measured through the internal wave gauge. Monochromatic tests with wave frequency f_w between 0.3 Hz and 0.7 Hz (spaced apart by 0.05 Hz), and wave height $H = 0.1, 0.15$ and 0.20 m have been used.

Viscous coefficient, $K_{v,i}$, which is the only uncertain parameter not known a priori, has been preliminary calibrated. Calibration of $K_{v,i}$ has been carried out using the datasets relative to $H = 0.15$ m and to the

different frequencies. Time-domain monochromatic simulations at different frequencies have been performed, using a set of values of $K_{v,i}$. For each simulation, the steady-state oscillating response is taken into account, and maxima/minima of the free surface oscillations above/below equilibrium ($z = 0$) are compared with experimental steady-state maxima/minima. The selected value of $K_{v,i}$ is the one that minimizes the mean difference between experimental and model points (i.e., maxima/minima at the different frequencies). In Figure 21.a, we report comparison of experimental oscillation amplitudes (with sign) with model outputs at different $K_{v,i}$ (a few values of the viscous coefficient are shown in the plot for better readability). The selected coefficient value is $K_{v,i} = 6.5$. This value is used throughout the other simulations.

In Figure 21.a-c we compare experimental oscillation amplitudes with calibrated model predictions for the different monochromatic sea states. Each plot refers to a different wave height. In the plots, we report amplitudes of upward ($z > 0$) oscillations (red points, magenta lines) and downward ($z < 0$) oscillations (blue points, cyan lines). Minima points are represented in the positive semi-plane to allow comparison of upward and downward oscillation amplitudes. Oscillation amplitudes are normalized with the wave amplitude, $A_w = H/2$, for comparison with Figure 3.b (that is, the design transfer function obtained with a fully-linear model).

The following observations can be drawn:

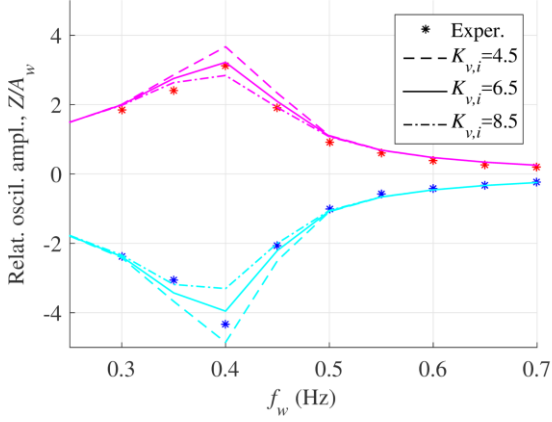
- Due to non-linearity (mainly, the geometric non-linearity introduced by the convergent divergent duct), upward and downward oscillation amplitudes are different.
- As H rises, the ratio of peak oscillation amplitude (at resonance) and wave amplitude decreases; that is, a saturation in oscillation occurs at large waves due to viscosity and other non-linearities.
- With respect to the previous prediction obtained with linear model, at design stage (dashed black curve in Figure 3.b), both experiments and the non-linear model feature smaller oscillation amplitudes, as a result of viscosity and non-linearities.
- In qualitative terms, the model efficiently captures all of the following effects: resonance frequency, wider downward oscillation, saturation of oscillation amplitude with increasing H .
- Mean difference between model points and experimental points is 14.1 % for upward oscillation amplitudes and 8.8 % for downward oscillation amplitudes (percentages are with respect to experimental values). The values are the average throughout the different sea states. Overall, the mean difference between model oscillation amplitudes and experimental oscillation amplitudes is 11.5 % of the experimental values.

It can be stated that the model meets expectations, as it captures all of the macroscopic phenomena involved in the collector dynamics, including the non-linear ones. Calibration of $K_{v,i}$ has proven to be efficient because, although it was carried out on a specific dataset ($H = 0.15$ m), it produced consistent results also at different wave heights. Numerical deviation of oscillation amplitude predictions from experiments is also good, considering the large number of underlying assumptions.

Calibrated model can be used to generate water column displacement (z) time-series to be compared with experiments. This is particularly useful to provide model assessment in irregular waves.

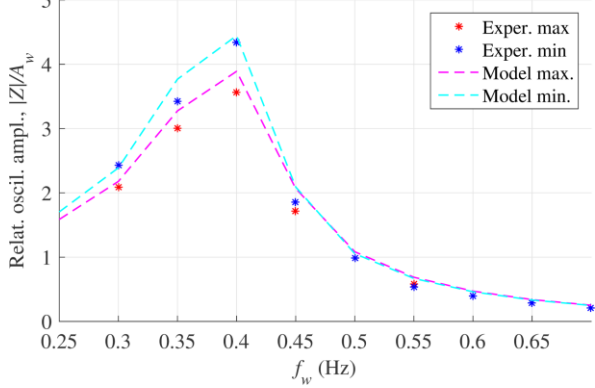
In Figure 22 we compare panchromatic wave time-series from experiments and model. Irregular waves simulations were performed using the undisturbed wave elevation in the far-field, measured by the wave gauges present in the tank. The undisturbed wave elevation is decomposed in a finite superimposition of harmonics using fast Fourier transform. The single harmonic components are then used to generate the excitation force profile.

Oscillation amplitudes - upward (max) and downward (min). $H=15$ cm



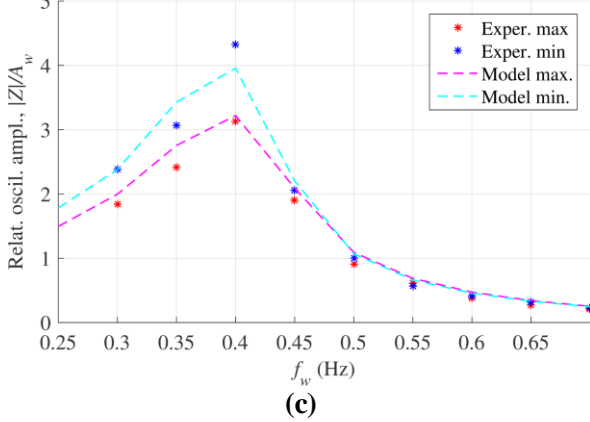
(a)

Oscillation amplitudes - upward (max) and downward (min). $H=10$ cm



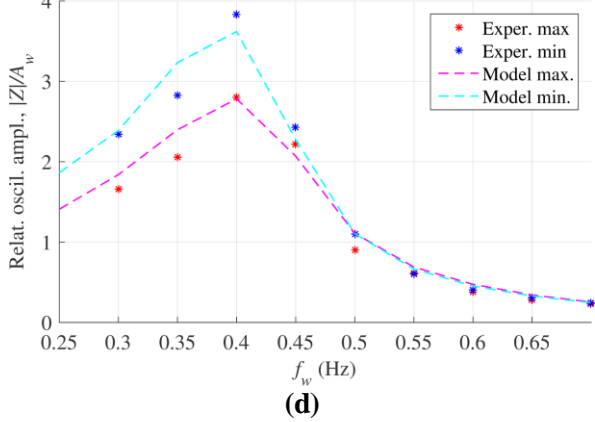
(b)

Oscillation amplitudes - upward (max) and downward (min). $H=15$ cm



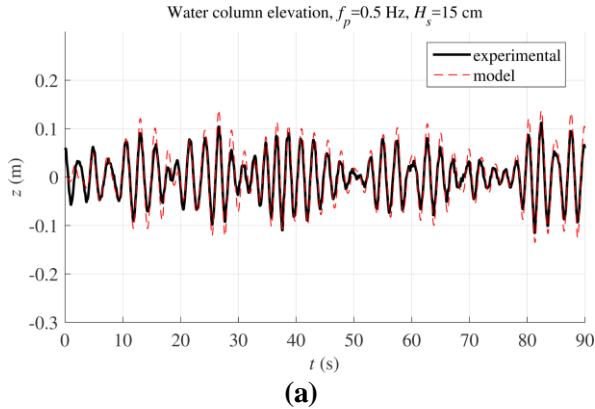
(c)

Oscillation amplitudes - upward (max) and downward (min). $H=20$ cm

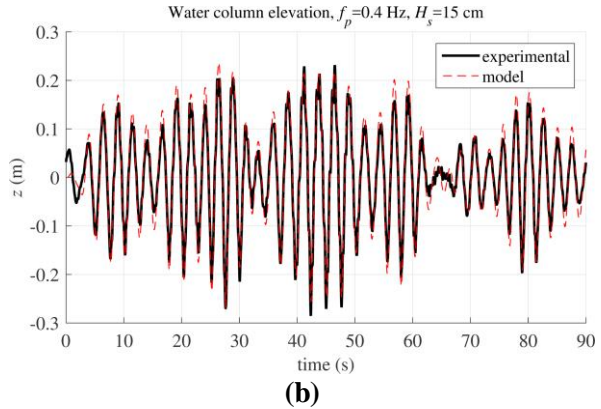


(d)

Figure 21. (a) Calibration of the viscous coefficient $K_{v,i}$: comparison of water column surface experimental max/min with the model. Points are for experiments, lines are for the model. Comparison of experimental and model free surface oscillation amplitudes (upward and downward) at different wave frequencies. Different plots are for different wave heights: (b) $H = 0.10$ m, (c) $H = 0.15$ m, (d) $H = 0.20$ m.



(a)



(b)

Figure 22. Comparison of water column free surface position time-series from experiments and models. The plots refer to panchromatic waves with Jonswap spectrum ($\gamma = 3.3$) with the following parameters: (a) $f_p = 0.5$ Hz, $H_s = 0.15$ m; (b) $f_p = 0.4$ Hz, $H_s = 0.15$ m.

4.2.2 U-OWC + DEG mechanical model validation

In a second step of the validation procedure, we couple the previously-validated hydrodynamic model with the mechanical CD-DEG model. At this stage, the purely elastic model of the CD-DEG is used (without electric activation), to validate the coupled hydro-elastic response of the device, i.e., verifying that the model catches the shift in resonance peak due to membrane rigidity, and the reduction in water column oscillation amplitude.

CD-DEG mechanical model makes use of VHB 4905 hyperelastic parameters (Table 1.a). The air chamber is considered adiabatic.

Consistently with hydrodynamic model validation, hydro-elastic model is validated against monochromatic wave tests using oscillation amplitudes of relevant variables, namely, free surface displacement, z , air chamber gauge pressure, Δp , and membrane tip height, h .

First, the CD-DEG is treated as an ideal non-viscous material, according to the model described in Sect. 4.1.2. In this scenario, CD-DEG model is coupled with the calibrated hydrodynamic model without need of further calibration or additional unresolved variables.

With reference to a DE membrane featuring $t_0 = 2$ mm and $\lambda_p = 3.39$, in Figure 23 we compare oscillation amplitudes of the mentioned variables. Capital letters in the plots stand for the magnitude of the oscillation amplitude. As in the purely hydrodynamic model, distinction is made between upward oscillation (i.e., maxima of the considered variables) and downward oscillation (i.e., minima of the considered variables, in module).

The plots show that the model captures experimental results fairly. In particular, it is capable of predicting the trend in oscillation amplitudes as a function of frequency. In general, the model overestimates oscillation amplitudes, especially air pressure and membrane tip elevation; instead, the model predicts free surface oscillation with a good level of agreement, comparable to that of Figure 21.b-d.

The observed mismatch is due to the relevant viscosity of VHB. As remarked in Sect. 2.1, VHB is highly visco-elastic, and it is only employed in the experimental tests because it is easy to handle and it is available in rolls of relatively large size that are suited for the implementation of large size DEGs. The ideal CD-DEG model described in Sect. 4.1.2 works for material with low hysteresis, as those envisaged for the full-scale application. In the present application, DE material viscosity should also be kept into account.

Although a rigorous consideration of visco-elasticity should make use of established visco-elastic models [3], [15], for the aim of capturing the effect of material dissipation in the present application, we have used a simplified approach. It has already been observed that plots in Figure 23 provide fair estimation of free surface oscillation, but they overestimate pressure and tip elevation. Additional dissipation should be then included within the DEG model. To do this, we introduce a linear DEG viscosity, B_p . Viscosity is here reduced to the membrane tip oscillation, h . Consequently, the DEG does not simply behave as a static component, and Eq. (21) (relating the air pressure to the DEG deformation and electric state) takes the following form:

$$\Delta p = \frac{4h}{h^2 + e^2} \frac{t_0}{\lambda^2} \left[\lambda \frac{\partial \Psi(\lambda_1, \lambda_2)}{\partial \lambda_1} \Big|_{\lambda_1 = \lambda_2 = \lambda} - \varepsilon E^2 \right] + B_p \dot{h} \quad (33)$$

Eq. (33) is a simplified model for the dissipative CD-DEG, in the most generic case in which electric activation is also present.

Parameter B_p needs calibration, which is carried out using the same procedure used for $K_{v,i}$ in the previous case. Upon selecting a value $B_p = 250$ kg/(m²s), model predicted oscillation compare to experiments as in Figure 24.

Compared to Figure 23, the dissipative DEG model provides an improvement of model agreement with experimental data. With reference to that case and to the plots in Figure 24, in Table 2 we resume the percentage discrepancies of model predicted oscillation amplitudes from experimental values. The agreement of the model with experiments is remarkable, as the mean discrepancy is below 10 %.

In analogy with hydrodynamic model validation, in the following we compare experimental time-series from panchromatic tests with those predicted by the model. Simulations have been run using experimental wave profiles (measured in the device far-field), which have been decomposed into a summation of harmonics through fast Fourier transform and have been used to generate model excitation force. Results are in Figure 25, where we compare free surface, air pressure, and membrane tip time-series for different panchromatic waves, featuring different wave parameters and peak enhancement factor. The plots refer to experiments with the same CD-DEG, featuring $t_0 = 2$ mm and $\lambda_p = 3.39$.

The plots confirm the very good agreement of the coupled model with the experiments: all of the time-series are well reproduced by the models, not only in terms of qualitative trend but also in terms of oscillation amplitudes matching. Adherence of model to panchromatic tests results confirm the model validity throughout the wave frequency range of interest.

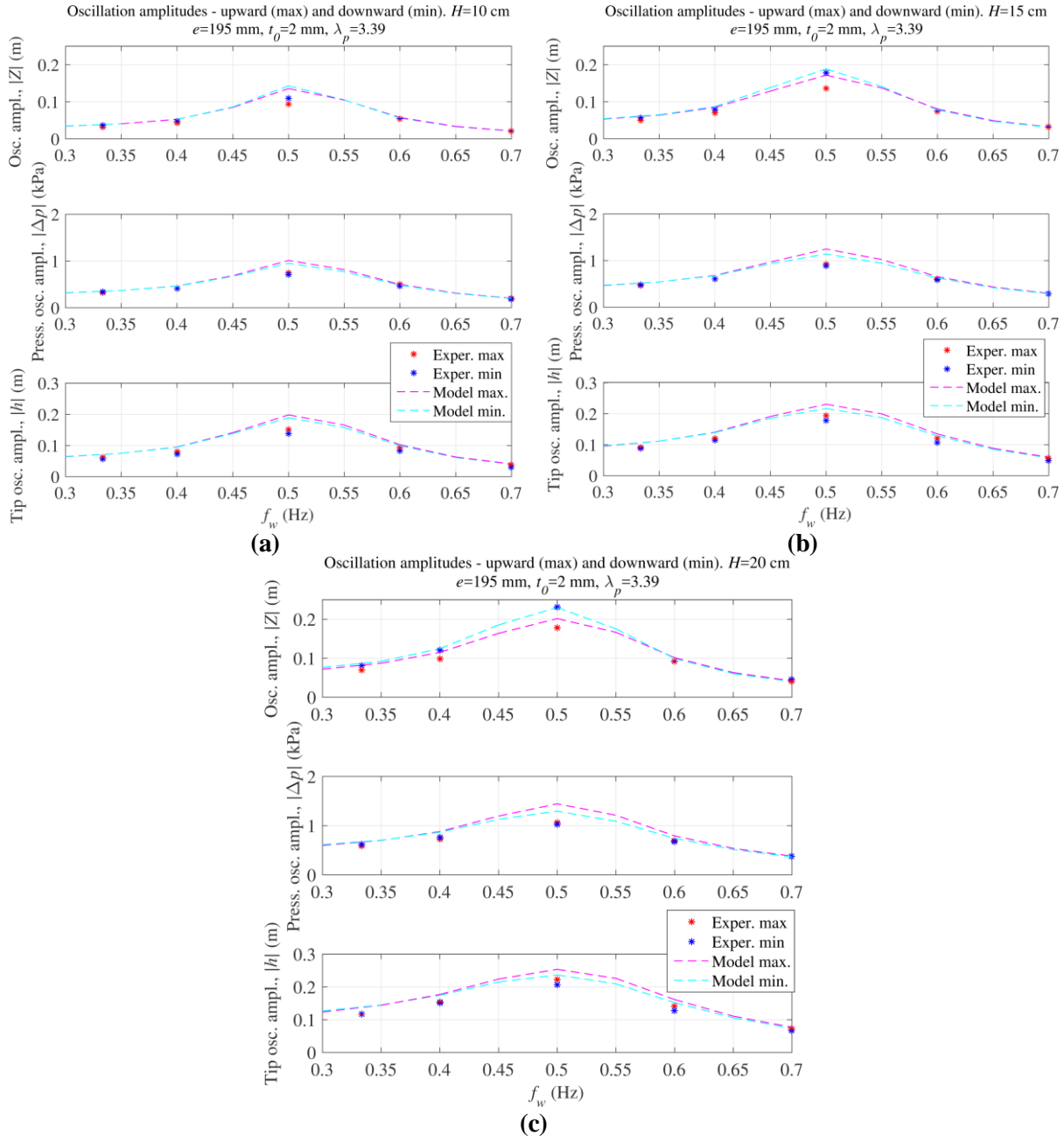


Figure 23. OWC collector + DEG model validation - Comparison of experimental and model oscillation amplitudes for the case with ideal non-dissipative DEG. Top subplots are for the free surface oscillation, middle subplots are for air pressure oscillations; bottom subplots are for membrane tip oscillation. The three plots are for different wave heights: (a) $H = 0.10\text{m}$, (b) $H = 0.15\text{m}$, (c) $H = 0.20\text{m}$.

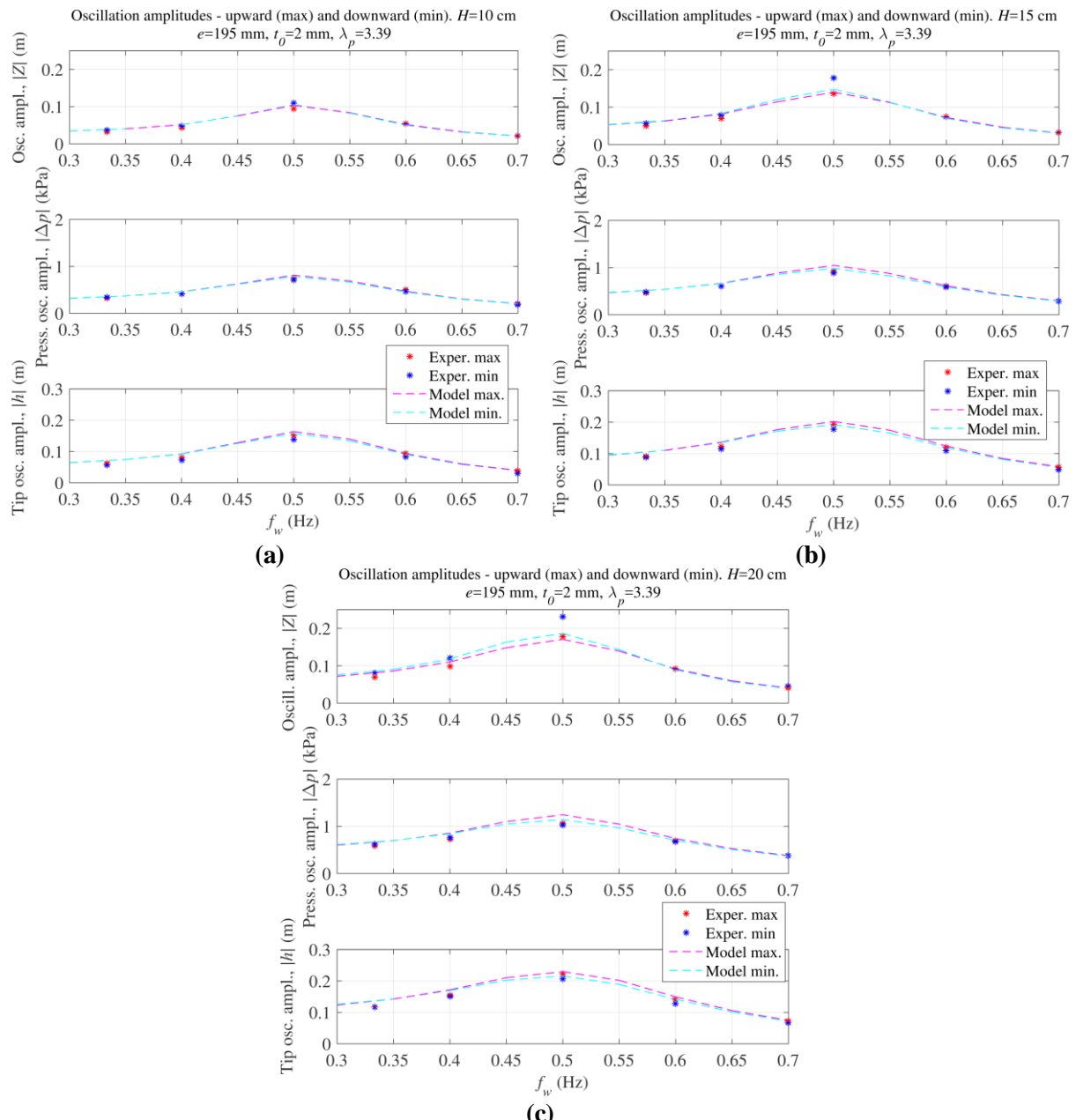


Figure 24. OWC collector + DEG model validation - Comparison of experimental and model oscillation amplitudes.
DEG dissipation is modelled by membrane damping, B_p . The three plots are for different wave heights: (a) $H = 0.10$ m, (b) $H = 0.15$ m, (c) $H = 0.20$ m.

Table 2. OWC collector + DEG mechanical model validation - Percentage mean difference between model predicted oscillation amplitudes and experimental values throughout the different sea states. Percentages are with respect to the experimental values. Distinction is made between maxima and minima of the oscillations.

	Upward oscill.	Downward oscill.
$ Z $	8.9 %	7.5 %
$ \Delta p $	9.1 %	6.3 %
$ h $	15.0 %	7.9 %

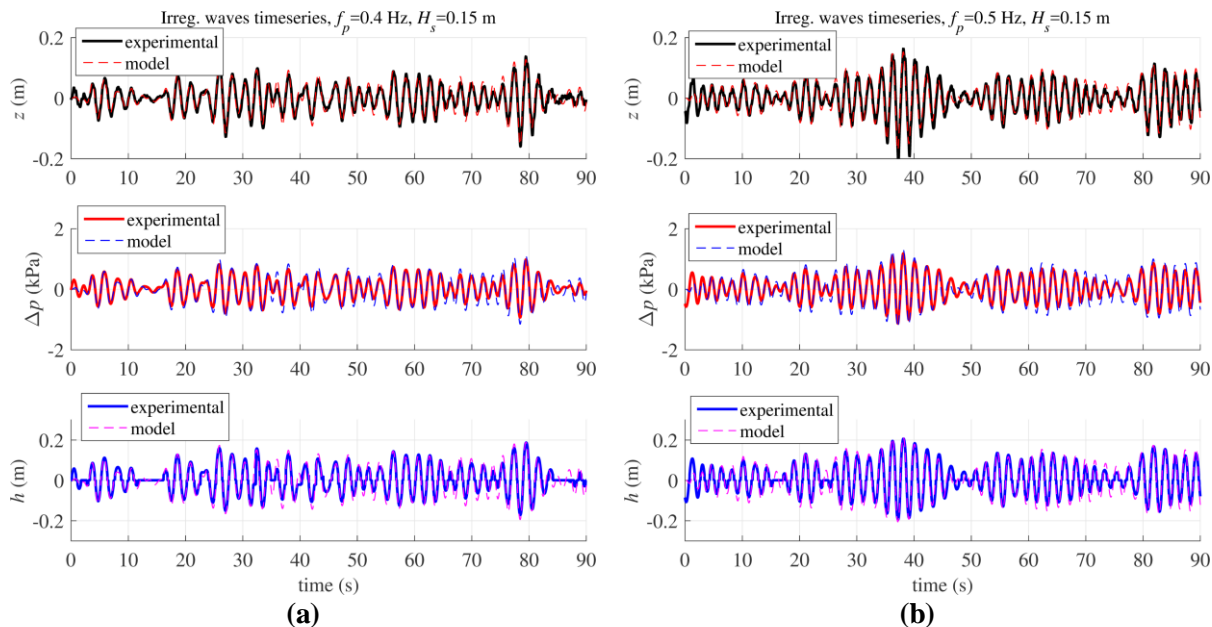


Figure 25. Comparison of relevant variables (z , Δp , h) time-series from experiments and models. The plots refer to panchromatic waves with Jonswap spectrum with the following parameters: (a) $f_p = 0.4$ Hz, $H_s = 0.15$ m, $\gamma = 3.3$; (b) $f_p = 0.5$ Hz, $H_s = 0.15$ m, $\gamma = 3.3$. Experimental membrane tip oscillation below a certain threshold (approx. 2 cm) are not visible, because the membrane was hidden by support flanges and could not be tacked by the camera.

4.2.3 Wave-to-wire hydro-electro-elastic model validation

In this section, the effect on electric activation on the device dynamics is included in the validation process, and the complete wave-to-wire WEC model is checked against experiments. The objective is to verify the agreement of both voltage variations on the DEG due to deformation and the effect of activation on relevant time-series (e.g., oscillation amplitude variations, effect of instantaneous activation).

At this stage of the validation, no further unknown parameters (that need calibration) are present. Previously validated hydro-elastic model is integrated with DEG electric response model and with a controller.

The level of electric load used in each experiment is parametrized through V_0 , i.e. the charging voltage on C_a (see Figure 5.a). Triggering of the various phases of the ECC is commanded by the same control block implemented in the Simulink scheme used to control the setup. The output of the control block is a square signal that returns 0 when the membrane should be inactive and 1 when the DEG should be electrically active. The voltage on the DEG at any instant is the product of the control signal times the voltage provided by Eq. (1).

Air pressure is used as control variable to generate the control signal. DEG charging/discharging is not instantaneous, as this would damage the circuitry, as explained in Sect. 2.3. These dynamics have been simulated by applying a first order linear system (with unitary gain and a pole at 63 rad/s) on the controller output signal, to smooth voltage rise/fall at charging/discharging.

Attention is thus focused on dynamics alteration due to electric activation. Differently from previous validation steps, we first report a comparison of relevant time-series before and after activation. To isolate the effect of electric activation, however, we restrict to consider monochromatic time-series.

With reference to four different sea conditions featuring same wave height ($H = 0.15$ m) and different frequency, in Figure 26 we compare experimental and model time-series of the following variables: water column free surface position, z , air gauge pressure, Δp , DEG tip height, h , DEG voltage, V . The plots refer to a DEG with the following features: $t_0 = 2$ mm, $\lambda_p = 3.39$, in parallel to a capacitance with $C_a = 394$ nF. Charging voltage on C_a is $V_0 = 6$ kV. The plots refer to a scenario in which the DEG is initially idle, and it is then activated after a certain amount of time.

Time-series show a remarkably good agreement between model and experiments. Most importantly, the model captures the following effects, which have also been discussed in Sect. 3.3:

- Instant activation provokes a sharp pressure drop. Although this drop is necessarily associated to a variation in membrane shape, the effect on tip height is not evident from the graph.
- Electric activation provokes either an increase or a reduction in the membrane oscillation amplitude, depending on the frequency (see the interpretation in Sect. 3.3).

Furthermore, the model fairly reproduces experimental voltage variations. In most cases, the voltage immediately after charging (at the beginning of each ECC) is underestimated by the model (i.e., the DEG capacitance is overestimated). In fact, the DEG capacitance strongly increases with increasing h . Therefore, a relatively small overestimate of tip height oscillations results in a perceptible overestimate of capacitance.

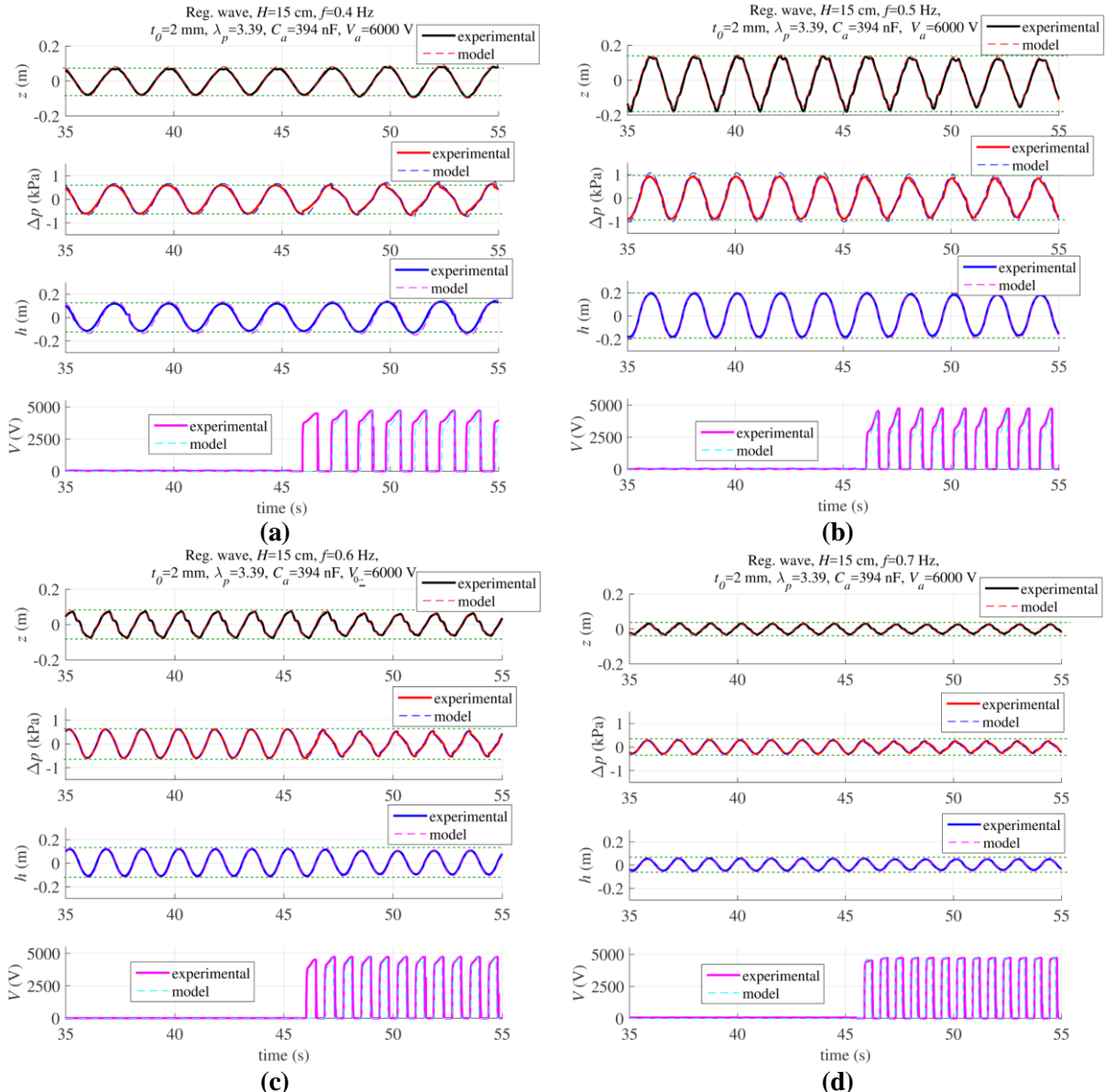


Figure 26. Comparison of relevant variables (z , Δp , h , V) time-series from experiments and models. Time-series represent tests in which the DEG is initially idle and is then activated. Green line in the first three subplots indicate oscillation amplitudes of the idle membrane, for comparison with oscillation amplitude after activation. The plots refer to regular waves with $H = 0.15$ m and the following frequencies: (a) $f_w = 0.4$ Hz, (b) $f_w = 0.5$ Hz, (c) $f_w = 0.6$ Hz, (d) $f_w = 0.7$ Hz.

In analogy with previous validation steps, in Figure 27 we compare modelled and experimental oscillation amplitudes (both upward and downward) of oscillating variables (z , Δp , h) in monochromatic waves.

Oscillation amplitudes refer to steady state oscillations in presence of electric activation. Plots refer to tests on a CD-DEG with $t_0 = 2$ mm, $\lambda_p = 3.39$, $C_a = 394$ nF and $V_0 = 6$ kV. A resume of percentage discrepancy of model oscillation amplitudes with respect to experimental ones in is Table 3. Results confirm the good agreement of the model with the experiments, with mean discrepancy of about 10 % with respect to the experimental value that is slightly larger than for the purely mechanical model validation.

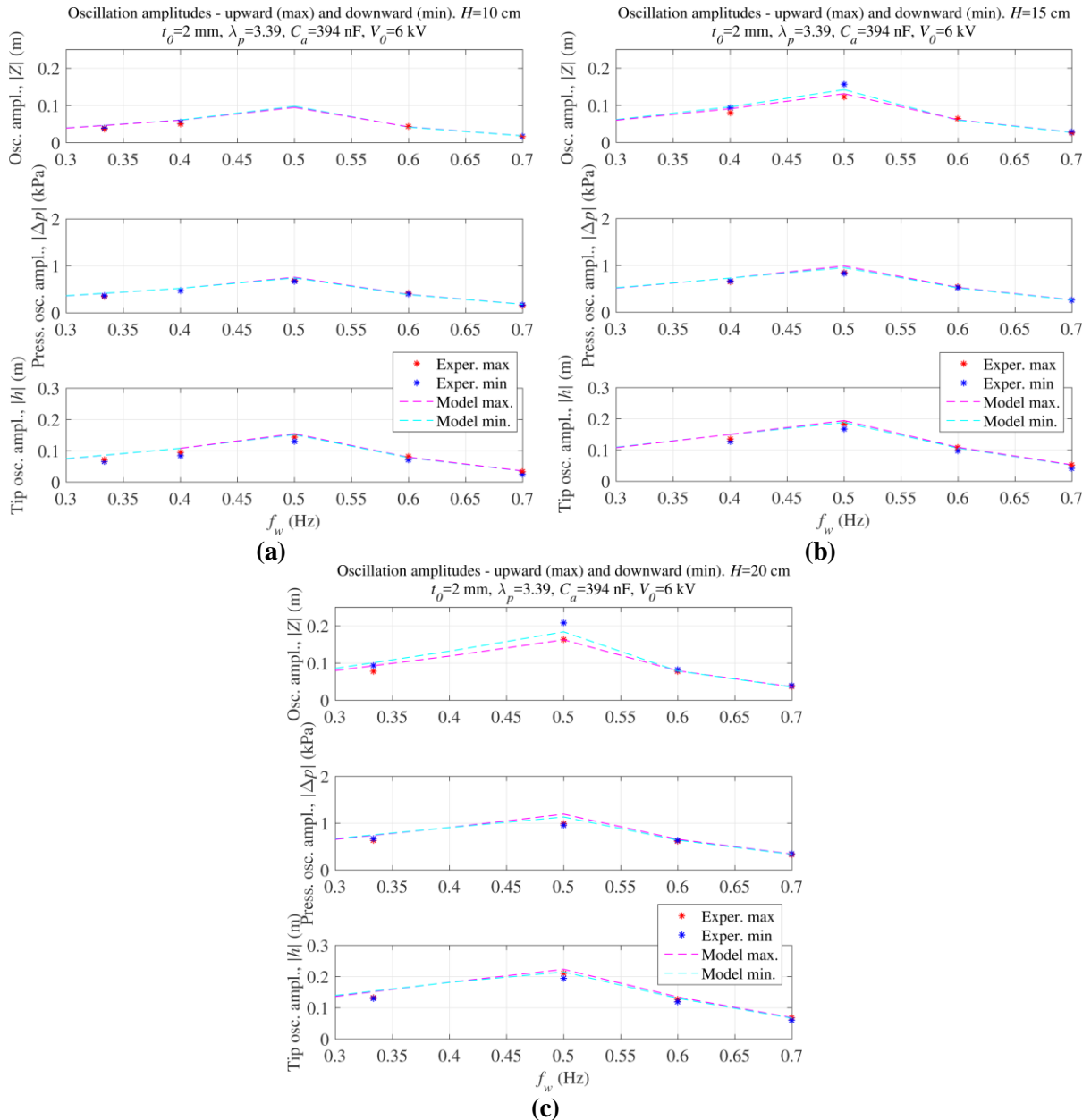


Figure 27. Wave-to-wire model validation - Comparison of experimental and model oscillation amplitudes, in presence of electric activation. Monochromatic wave heights for the different plots are: (a) $H = 0.10$ m, (b) $H = 0.15$ m, (c) $H = 0.20$ m.

Table 3. Wave-to-wire model validation - Percentage mean difference between model predicted oscillation amplitudes and experimental values throughout the different sea states. Percentages are with respect to the experimental values. Distinction is made between maxima and minima of the oscillations.

	Upward oscill.	Downward oscill.
$ Z $	9.7 %	8.6 %
$ \Delta p $	10.3 %	8.6 %
$ h $	7.8 %	17.4 %

4.2.4 Collector + DEG + open air chamber model validation

In this section, we provide validation of the open air chamber model presented in Sect. 4.1.3 with reference to exceptional sea conditions and security mode operation.

The hydro-elastic mechanical Poly-U-OWC model is coupled with the open air chamber dynamic model, and results are validated against survivability tests results (Sect. 3.4). Survivability tests have been carried out in absence of electric activation; therefore, in this analysis purely mechanical models are employed.

Validation is carried out using a dataset featuring constant monochromatic wave height $H = 25$ cm (i.e., a very energetic sea state, representative of extreme sea conditions) and different wave frequencies, with an orifice of 35 mm diameter on the air chamber. Upon calibration, the coefficient of discharge has been set to $C_v = 0.4$ (i.e., a comparable value with respect to literature reference values of discharge coefficients [16]). Comparison of experimental and theoretical oscillation amplitudes of relevant physical variables are in Figure 28.a.

The model features an acceptable agreement with the experiments. Remarkably, it captures the shift in resonance frequency due to the aperture in the air chamber. Peak oscillation frequency results in 0.45 Hz (instead of 0.5 Hz) due to stiffness reduction induced by the orifice aperture.

Comparison of model and experiments time-series for one of the monochromatic sea states in exam are in Figure 28.b. The plots show that, besides capturing the oscillation amplitudes fairly well, the model captures the non-linearity in water column free-surface oscillation, whose time profile has non-sinusoidal shape.

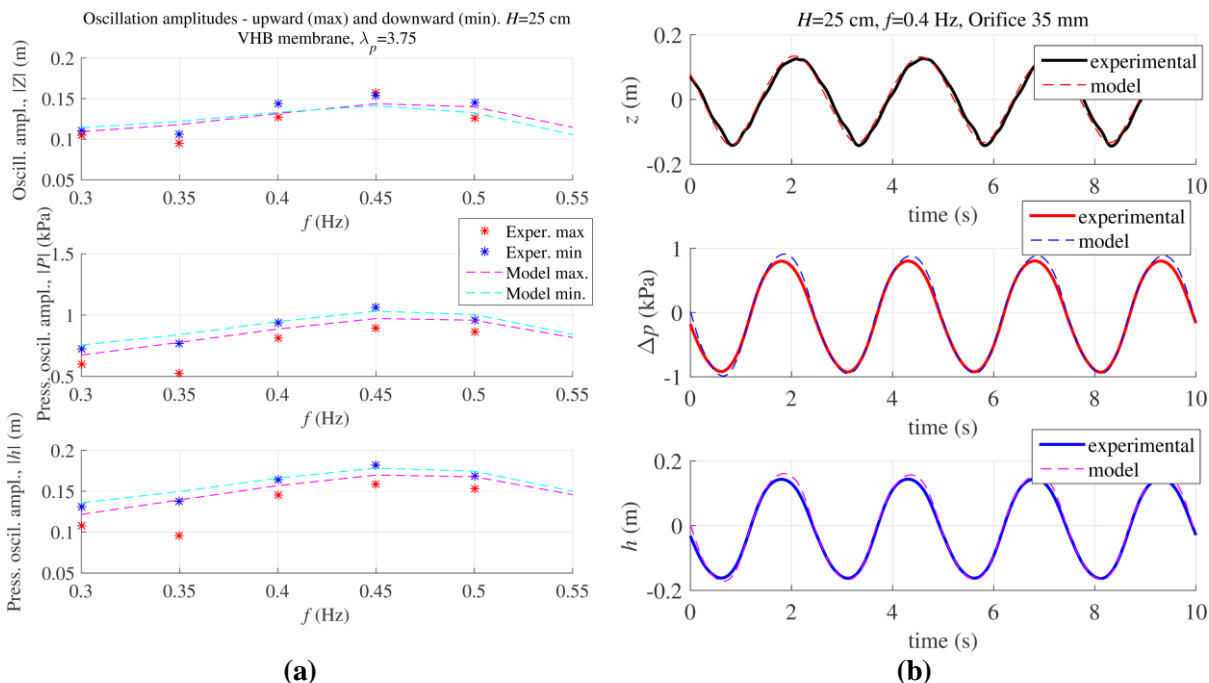


Figure 28. Poly-U-OWC with open air chamber (security mode) model validation: (a) Comparison of experimental and model oscillation amplitudes in presence of large monochromatic waves with $H = 0.25$ m and different frequencies. (b) Relevant time-series (z , Δp , h) for a regular sea state with $H = 0.25$ m and $f_w = 0.4$ Hz. Both pictures refer to an orifice aperture of 35 mm diameter in the air chamber.

5. CONCLUSIONS AND FUTURE WORKS

5.1 Conclusions

This deliverable describes the results of a test campaign conducted on a novel DEG-WEC developed within the framework of the project PolyWEC.

The designed WEC is based on the concept that is described in detail in D3.3. The proposed system is an OWC with a fixed U-shaped axisymmetric collector that increases the added mass and the wave energy capture of the device. The system is named Poly-U-OWC.

The developed model prototype has provided a further scale-up step with respect to previous tests (described in D4.1 and D4.2), increasing the scale of the device to 1:25/1:30. The developed system, as in the previous flume tests, is a WEC with many of the operational abilities of a real-scale system. Specifically, the prototype is able to actually convert wave power into electrical energy with a power output in the range of 2-6 Watts.

The experiments include tests in operational and exceptional sea conditions including tests with combined wave-current loads. The test campaign was conducted at the Flowave test facility (in Edinburgh) in two different sessions.

In a first test session, the system has been characterized against monochromatic wave loads with periods in a range of 1.4 s - 3 s (frequency 0.3-0.7 Hz) achieving the milestone of a maximum converted power of more than 3.8 W.

In further sessions, panchromatic tests have been conducted which make it possible to verify the energy conversion in testing conditions which are closer to real sea-states. Additionally, during panchromatic tests, preliminary control strategies have been tested and tuned, thus demonstrating the possibility of controlling the system using a very simple approach. Such a control strategy is exclusively based on the acquisition of the pressure inside the chamber and the evaluation of its derivative, with no need for predictions of the incoming waves.

Besides these two main results, the obtained measurements make it possible to:

- Tune and validate the models: complex models that couple the hydrodynamic response with non-linear hyperelastic models of the PTO have been successfully tuned (with particular reference to viscosity parameters) and verified against a vast amount of experimental data;
- Verify the design approach and assumptions: the validation of models makes it possible to verify the design approach and assumptions (for example the scaling rules) that has been assumed and presented in deliverable D3.4;

Additional tests were conducted in exceptional wave conditions including extreme waves (having the system inactive) and combined wave and currents loads. This made it possible to:

- Verify the reduced sensibility of the system to currents: this is a feature that was rather expected since the system is a bottom fixed OWC and it is highly tolerant to current loads;
- Validate a possible depowering strategy/concept, based on a relief valve, that is able to improve survivability of the device in extreme wave conditions.

5.2 Future testing works

The developed experimental campaign made it possible to verify several of the characteristics of the proposed Poly-U-OWC. However, several aspects are still to be investigated specifically:

(1) Scalable conversion electronics: the tests that were reported in this deliverable have been conducted with a simplified electronics that implements representative energy generation cycles but presents limits in the upscaling. One of the most crucial steps, among future activities, will be the development of a new version of the power electronics whose topology is clearly scalable up to the range of hundreds of kilowatts. Such a topology for the power electronics has been already designed and it is currently being developed under the project WETFEET (funded by European Union's Horizon 2020 research and

innovation programme under G.A. No 641334), that includes a work-package that aims at the continuation of the work conducted in the project PolyWEC.

The development of such an electronics together with an upscaled test-bench setup will also make it possible to verify the optimal control strategies envisaged in D3.4 with hardware in the loop tests.

(4) Floating version of the Poly-U-OWC. A floating conversion unit is probably the most promising solution, since floating systems can be, by nature, arranged in large arrays. The design of a floating system concept is currently in the roadmap of future activities to be conducted as continuation of the PolyWEC project.

Besides these aspects that are related to the PTO operational test, further experimental investigations should be oriented to the characterization of the long term operation of DEG with additional effort in material fatigue testing and characterization. Additionally, it is necessary to study and develop a custom/scalable manufacturing strategy for DEG-PTOs, capable to provide high repeatability, precise geometrical tolerances, and defect free materials.

REFERENCES

- [1] Forehand, D., Richon, J. B., Fontana, M., Moretti, G., Rosati Papini, G. P., Vertechy, R. PolyWEC Deliverable D4.1 - Wave-tank tests of first generation PolyWEC units, 2016.
- [2] M. Fontana, R. Vertechy, G. Moretti, D. Forehand, and D. Ingram, "PolyWEC Deliverable D1.1 - Architectures and material-property specifications for first- and second- generation PolyWECS," 2013.
- [3] Vertechy, R., Rosati, G. P. P., & Fontana, M. (2015). Reduced model and application of inflating circular diaphragm dielectric elastomer generators for wave energy harvesting. *Journal of Vibration and Acoustics*, 137(1), 011004.
- [4] Moretti, G., Daniele, L., Fontana. M., Vertechy. R., Forehand, D. (2016). PolyWEC Deliverable D3.3 - Second iteration prototypes of first and second generation devices.
- [5] Keplinger, C., Li, T., Baumgartner, R., Suo, Z., & Bauer, S. (2012). Harnessing snap-through instability in soft dielectrics to achieve giant voltage-triggered deformation. *Soft Matter*, 8(2), 285-288.
- [6] Berselli, G., Vertechy, R., Vassura, G., & Parenti-Castelli, V. (2011). Optimal synthesis of conically shaped dielectric elastomer linear actuators: design methodology and experimental validation. *IEEE/ASME Transactions on Mechatronics*, 16(1), 67-79.
- [7] Shian, S., Huang, J., Zhu, S., & Clarke, D. R. (2014). Optimizing the electrical energy conversion cycle of dielectric elastomer generators. *Advanced Materials*, 26(38), 6617-6621.
- [8] Noble, D., Davey, T., Steynor, J., Bruce, T., Smith, H., & Kaklis, P. (2015, April). Wave-current interactions at the FloWave Ocean Energy Research Facility. In EGU General Assembly Conference Abstracts (Vol. 17, p. 4821).
- [9] B. Teillant, I. Machado, M. Vicente, P. Chainho, M. Fontana, R. Vertechy, G. Moretti, C. Thomson, G. Harrison, Deliverable D4.1 - Preliminary assessment and exploitation of PolyWECS, 2017.
- [10] Moretti, G., Daniele, L., Fontana. M., Vertechy. R., Forehand, D. (2016). PolyWEC Deliverable D3.4 - Best-Practice guidelines for the design and control of PolyWEC devices.
- [11] Viuff, T. H., Andersen, M. T., Kramer, M., & Jakobsen, M. M. (2013). Excitation forces on point absorbers exposed to high order non-linear waves. In 10th Ewtec 2013 European Wave and Tidal Energy Conference Series. Technical Committee of the European Wave and Tidal Energy Conference.
- [12] G. Moretti, R. Vertechy, G. P. Rosati Papini, M. Fontana, D. Forehand, and M. Alves, "PolyWEC Deliverable D1.2 - Novel non-linear multi-physics continuum models," 2015.
- [13] Holzapfel, G. A. (2000). Nonlinear solid mechanics (Vol. 24). Chichester: Wiley.
- [14] Falcao, A. D. O., & Justino, P. A. P. (1999). OWC wave energy devices with air flow control. *Ocean Engineering*, 26(12), 1275-1295.
- [15] Bortot, E., Denzer, R., Menzel, A., & Gei, M. (2016). Analysis of viscoelastic soft dielectric elastomer generators operating in an electrical circuit. *International Journal of Solids and Structures*, 78, 205-215.
- [16] Hollingshead, C. L., Johnson, M. C., Barfuss, S. L., & Spall, R. E. (2011). Discharge coefficient performance of Venturi, standard concentric orifice plate, V-cone and wedge flow meters at low Reynolds numbers. *Journal of Petroleum Science and Engineering*, 78(3), 559-566.
- [17] Moretti G, Rosati G, Alves M, Grases M, Vertechy R, Fontana M. Analysis and Design of an Oscillating Water Column Wave Energy Converter With Dielectric Elastomer Power Take-Off. ASME. International Conference on Offshore Mechanics and Arctic Engineering, *Volume 9: Ocean Renewable Energy*